

# Noise generation by turbulence-propeller interaction in asymmetric flow

ROSALYN A. V. ROBISON<sup>1,2</sup>, N. PEAKE<sup>1†</sup>

<sup>1</sup>Department of Applied Mathematics and Theoretical Physics, University of Cambridge, Wilberforce Rd, Cambridge CB3 0WA, UK

<sup>2</sup>Current address: Global Sustainability Institute, Anglia Ruskin University, East Rd, Cambridge CB1 1PT, UK

(Received ?; revised ?; accepted ?. - To be entered by editorial office)

This paper is concerned with a particular source of both broadband and tonal aeroengine noise, termed *Unsteady Distortion Noise* (UDN). UDN arises from the interaction between turbulent eddies, which occur naturally in the atmosphere or are shed from the fuselage, and the rotor. This interaction produces broadband noise across a broad frequency spectrum. In cases in which there is strong streamtube contraction, which is especially true for open rotors at low-speed conditions (such as at take-off or for static testing), tonal noise at frequencies equal to multiples of the blade passing frequency are also produced, due to the enhanced axial coherence caused by eddy stretching. In a previous paper (S.J. Majumadar & N. Peake 1998 *J. Fluid Mech.* **359**, 181-216), a model for UDN was developed in axisymmetric flow. However, asymmetric situations are also of much interest, and in this paper we consider two cases of asymmetric distortion, firstly that induced by the proximity of a second rotor, and secondly that caused by non-zero inclination to the flight direction, as found at take-off. This requires significant extension of the previous axisymmetric analysis. We find that the introduction of asymmetric flow features can have a significant decibel effect on the radiated sound power. For instance, in low-speed conditions we find that the tonal level is reduced significantly by the proximity of a second rotor, compared to the axisymmetric case, while the effect on the broadband levels is rather modest.

---

## 1. Introduction

There is currently considerable interest in the future of the open rotor aeroengine (also known as the Counter-Rotating Open Rotor (CROR), the Advanced Open Rotor (AOR), the advanced turboprop, the Counter-Rotating Propfan (CRP), or simply the propfan), which is predicted to deliver fuel savings of at least 30% compared to current turbofans Smith (1985), and 10-20% savings compared to next-generation turbofans. Open rotor driven aircraft can operate efficiently at cruise speeds of up to Mach 0.8, and are therefore suitable candidates for commercial medium- and short-haul flights. However, the level and type of noise generated by the open rotor was a significant factor in commercial development being abandoned a decade after the technology first emerged in the 1980s. Research into many areas of open rotor aeroacoustics has now been resumed, with the aim of meeting current and future noise certification criteria.

Several different noise sources must be considered for the open rotor (see a recent review by Peake & Parry (2012)), but in this paper we are concerned with just one

† Email address for correspondence: n.peake@damtp.cam.ac.uk

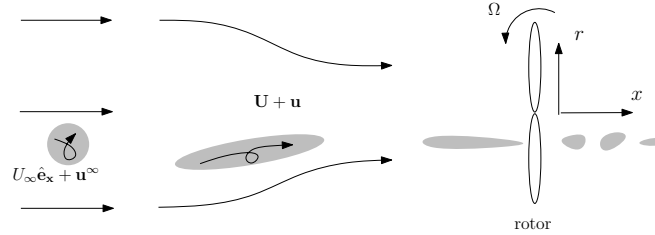


Figure 1: Representation of the Unsteady Distortion Noise mechanism, whereby turbulent eddies are stretched and then ‘chopped’ by the rotating engine blades. The various mean and turbulent velocities used throughout this paper (see §2.1) are also illustrated.

source, so-called Unsteady Distortion Noise (UDN). UDN arises from the interaction between atmospheric turbulence (or turbulence from some part of the aircraft fuselage upstream) and the rotor blades (see Figure 1), and is of particular relevance to the large, unducted, open rotor. The basic mechanism for UDN generation was determined in pioneering experimental work by Hanson (1974) and Cumpsty & Lowrie (1974): turbulent eddies are stretched axially by the streamtube contraction into the rotor, and are then chopped many times by adjacent blades at the same location to provide coherent forcing, leading to both tonal and broadband noise. Models for noise generation by turbulence-blade interaction are well-known and long-standing, e.g. Sharland (1964), Mani (1971), Homicz & George (1974), and we mention in particular here Amiet (1975) and Paterson & Amiet (1982), who developed a foundational model for the far-field noise due to a single flat-plate airfoil in terms of the turbulent energy spectrum and the airfoil response function. In these models the turbulence is not distorted by the (uniform) mean flow as it convects towards the airfoil. However, we stress here that it is the distortion induced by the rotor flow which is the defining feature of the generation of UDN, and several models for this have been developed. Hanson himself used a statistical distribution of discrete eddies, and assumed each eddy acted as a point force on the blade in the radial direction. In his framework the lift pulse due to an eddy and the joint probability density functions for the turbulent eddy characteristics must be specified as inputs. Hanson (2001) has also developed a method whereby random offset times within turbulent velocities can be used to represent inhomogeneity.

In a pair of papers (Simonich *et al.* (1990), Amiet *et al.* (1990)) a full UDN prediction method was set out in the context of a helicopter rotor. This involved the solution of a series of model problems, to calculate:

- (a) the distortion of the incident turbulence by the non-uniform flow, crucially allowing for the differential drift between particles on neighbouring streamlines, using Rapid Distortion Theory (RDT), see Hunt (1973), Goldstein (1978*b*);
- (b) the interaction of the distorted turbulence with the blades to generate unsteady lift, in their case neglecting cascade interactions between adjacent blades;
- (c) the sound radiated to the far field by the unsteady blade lift forces.

Cargill (1993) suggested this same approach in the open rotor context, and his framework was developed in detail in Majumdar & Peake (1998) for a rotor in *axisymmetric* mean flow. The aim of the present paper is to extend Majumdar & Peake’s analysis to the case of UDN generated by an open rotor in *asymmetric* mean flow. Although the assumption of axisymmetry is often a reasonable one, there are a number of practical cases in which an open rotor may operate in strongly asymmetric flow, and in this paper we consider two specific asymmetric configurations. The first considers two adjacent rotors, or equivalently a single rotor mounted next to a wall as an approximate model for the presence of

the fuselage. Indeed, the effect of the fuselage on the flow ingested into an open rotor may be significant when the open rotor is mounted in the ‘pusher’ configuration at the rear of the aircraft. Our second form of asymmetric mean flow model is that of a rotor whose axis is at a non-zero angle to the flight direction, i.e. at *incidence*. In reality, most aeroengines operate at incidence for some periods during flight, incidence typically being highest during take-off. Incidence is greater when the open rotor is mounted in the ‘puller’ configuration due to the proximity of the wing, and furthermore open-rotor powered aircraft can climb and descend more steeply than equivalent turbofan-powered aircraft (high blade stresses being a limiting factor for the latter), which also increases incidence.

We wish to draw attention here to a recent important UDN experiment, Alexander *et al.* (2013), and associated theoretical model, Glegg *et al.* (2013), which is related to our work. The situation these authors consider is of a rotor operating close to a wall and partially submerged in the thick wall boundary layer. Inhomogeneous turbulence in the boundary layer interacts with the rotor, to generate UDN. The theoretical model, Glegg *et al.* (2013), differs from our approach in two key respects; first, to account for the boundary layer they allow for the presence of mean shear upstream; and second, their blade interaction and noise calculations are based in the time, as opposed to the frequency, domain. Turning first to the issue of mean shear, we note that the RDT of Hunt and Goldstein, as applied in Majumdar & Peake (1998), in the current paper, and in Glegg *et al.* (2013), is only valid for potential base flows. Here, and in Majumdar & Peake (1998), we consider mean flows generated by actuator disks, in which the mean vorticity is either bound to the disks or confined within their wakes, with the effect that the distortion of turbulence from upstream occurs in potential mean flow, to which RDT is applicable. In contrast, in Glegg *et al.* (2013) the presence of the mean boundary layer strictly invalidates the use of potential-theory RDT (although the key qualitative feature of strong streamtube contraction into the rotor is no doubt captured). Another feature of the model problems we consider is that far upstream the mean flow is uniform, allowing the far-upstream turbulence to be treated as a superposition of simply-convected harmonic gusts; in contrast, Goldstein (1978*a*) has shown that in the presence of mean shear the allowed convected gusts take a much more complicated form. This issue has recently been studied by Ayton & Peake (2014), who consider the gust distortion and noise generation by a thick aerofoil located in mean shear.

The second difference between the Glegg *et al.* (2013) approach and our own lies in their use of the time domain for the turbulence-blade interaction and noise calculations (see Glegg *et al.* (2014) for further details), whereas we work in the frequency domain throughout. It seems to us that both approaches have their merits. The time domain calculation certainly avoids the sort of time-consuming Bessel function summation which is a feature of the frequency domain analysis. On the other hand, in the problems we consider in this paper the frequency domain approach has the advantage of directly relating the energy spectrum of isotropic turbulence, which is very well known, to the frequency spectrum of the far-field noise, which is of course an object of much engineering interest. Equally, if one did not have a known spectrum far upstream, but instead had measurements of correlation functions near the rotor face, as in the experiments of Alexander *et al.* (2013), then the time domain approach could well be more natural. Another point of comparison between time-domain and frequency-domain approaches comes from the issue of source compactness and retarded-time variations. In compact, typically low and medium speed, cases the retarded-time variations over the source are small, and can be handled conveniently within the time-domain Ffowcs Williams and Hawkings equation (Ffowcs Williams & Hawkings 1969). However, for non-compact sources the retarded-

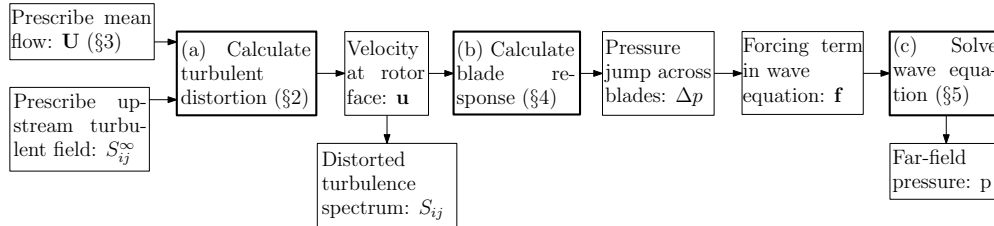


Figure 2: Schematic of the inputs to and outputs from our model. Computational steps are shown in boxes with thicker borders.

time calculations become more involved, especially at transonic and supersonic speeds when the retarded time may become multi-valued and the Doppler factors appearing in the denominator of the integrand in the Ffowcs Williams and Hawkings equation require special care. In the frequency domain these features are encoded within the coefficients of the Bessel expansions, and it is our opinion that this is a more convenient approach for high-speed flow. Finally, we wish to make the point that existing theories for predicting the distortion of the incident turbulence by the mean flow (RDT in potential flow, and the approach of Goldstein (1978*a*) and Ayton & Peake (2014) for shear flow) are set in the frequency-domain, but it may well be that time-domain analogues could be developed, and this would be an interesting area of further work.

Our basic methodology follows the steps set out at the start of the previous paragraph, see Figure 2. In §2 we describe the use of RDT to calculate the distortion of upstream isotropic turbulence as it propagates through our model asymmetric base flows (§3). The unsteady pressure distributions across the rotor blades are then calculated (§4), and used as the forcing term in the far-field wave equation to produce the final noise spectrum predictions (§5). Throughout our aim is to assess the effects of flow asymmetry on the radiated noise.

## 2. Distortion of turbulence

### 2.1. Rapid Distortion Theory, basic result

Rapid Distortion Theory (RDT) (see (Goldstein 1978*b*), (Hunt 1973)) is concerned with calculating the change in a small velocity perturbation  $\mathbf{u}$  as it is convected downstream by a dominant, distortive, potential mean base flow,  $\mathbf{U}$  (in our case, the streamtube contraction induced by the rotor) as shown in Figure 1. In what follows we choose the  $x$  axis to be aligned with the steady flow far upstream (so that  $\mathbf{U} \rightarrow U_\infty \hat{\mathbf{e}}_x$  as  $x \rightarrow -\infty$ , and  $U_\infty$  is the flight speed of the aircraft). The turbulent component of the velocity is denoted by  $\mathbf{u}$  and  $\mathbf{u} \rightarrow \mathbf{u}^\infty$  as  $x \rightarrow -\infty$ .

We consider the incident turbulence at upstream infinity to be composed of a distribution of individual unsteady harmonic gusts, which can be combined to give the full spectrum. Taking just a single such gust, the velocity of this gust at upstream infinity takes the form

$$u_i^\infty(\mathbf{x}) = a_i \exp\{i\mathbf{k} \cdot (\mathbf{x} - U_\infty t \hat{\mathbf{e}}_x)\}, \quad (2.1)$$

with  $\mathbf{a}$  a constant vector. Here,  $\mathbf{k}$  is the phase vector associated with this single gust; the full turbulence spectrum is obtained by integrating over all possible  $\mathbf{k}$ . We emphasise that in this subsection we consider a single incident gust component (2.1), but in the rest of the paper  $\mathbf{u}(\mathbf{x}, t)$  will refer to the total unsteady velocity, which is obtained by integrating over a spectrum of such gusts.

Following Goldstein (1978*b*), Majumdar & Peake (1998) were able to calculate the approximate distorted velocity perturbation resulting from this single gust condition upstream. Full details are given in Majumdar & Peake (1998), and we need only state their result here: the distorted gust is given approximately by

$$u_i(\mathbf{x}, t) = A_{ij} a_j \exp\{i\mathbf{k} \cdot (\mathbf{X} - U_\infty t \hat{\mathbf{e}}_x)\}, \quad (2.2)$$

where

$$A_{ij} = \left( \delta_{im} - \frac{l_i l_m}{|\mathbf{l}|^2} \right) \frac{\partial X_j}{\partial x_m}, \quad (2.3)$$

and

$$l_i = k_m \frac{\partial X_m}{\partial x_i}, \quad (2.4)$$

is the distorted wave-vector. The vector  $\mathbf{X} = X\hat{\mathbf{e}}_x + Y\hat{\mathbf{e}}_y + Z\hat{\mathbf{e}}_z$  is defined by Goldstein to have the properties

$$\frac{D_0}{Dt}(\mathbf{X} - U_\infty t \hat{\mathbf{e}}_x) = 0 \quad \text{and} \quad \mathbf{X} \rightarrow \mathbf{x} \quad \text{as} \quad x \rightarrow -\infty, \quad (2.5)$$

where  $D_0/Dt$  is the convective derivative for the steady base flow  $\mathbf{U}$ . Condition (2.5) is a statement that the three quantities  $X - U_\infty t$ ,  $Y$  and  $Z$  remain constant when moving with the mean flow. By labelling each steady streamline uniquely by its  $y$  and  $z$  coordinates far upstream and then, for every point along that streamline, defining  $Y$  and  $Z$  to be these upstream values, we can always satisfy this condition for  $Y$  and  $Z$ . The third quantity,  $X$ , is defined by  $X = U_\infty \Delta$ , where  $\Delta$  is the drift function, Lighthill (1956),

$$\Delta(\mathbf{x}) \equiv \frac{x}{U_\infty} + \int_{-\infty}^x \left[ \frac{1}{(U_\infty + U_x)} - \frac{1}{U_\infty} \right] dx', \quad (2.6)$$

where  $U_x = \mathbf{U} \cdot \hat{\mathbf{e}}_x$  and the path of integration is taken along the mean flow streamline.

In (2.2) we see that the nonuniform mean flow has the effect of modifying both the phase and the velocity of the gust. The distorted phase is  $\mathbf{k} \cdot \mathbf{X}$ , to be compared to the phase at upstream infinity,  $\mathbf{k} \cdot \mathbf{x}$ . The vector  $\mathbf{X}$  expresses the location from which a given fluid particle originated far upstream, through the components  $Y, Z$ , and the time taken for that fluid particle to reach its current location, through the component  $X$ . Note that  $\mathbf{X}$  is different from the position vector  $\mathbf{x}$ , except in uniform mean flow when  $\mathbf{X} = \mathbf{x}$ . The gust velocity is distorted through the action of the tensor  $A_{ij}$  defined in (2.3). The first term in (2.3),  $\partial X_j / \partial x_i$ , corresponds to the tilting of the gust velocity due to the changing orientation of material surfaces in the fluid as they propagate downstream (see Goldstein (1978*b*) for full details). The second term in (2.3) arises from the hydrodynamic potential field which accompanies the propagating vortical gust in order to conserve mass; this potential field depends on the vector  $\mathbf{l}$ , which is to be interpreted as the effective local wave vector, i.e.  $\mathbf{l}$  is the  $\mathbf{x}$  derivative of the local phase  $\mathbf{k} \cdot \mathbf{X}$ .

The approximation used by Majumdar (1996) in deriving equation (2.2) involves neglecting terms of order  $\partial^2 X_j / \partial x_i \partial x_i$  in favour of terms of order  $k_l (\partial X_j / \partial x_i) (\partial X_l / \partial x_j)$ . This is a reasonable approximation since, in cases of low distortion,  $\partial^2 X_j / \partial x_i \partial x_i$  is close to zero, while in cases of high distortion  $\partial X_j / \partial x_i$  is large (note also that although the approximation might fail in cases in which the  $k_l$  are all close to zero, such cases do not contribute significantly to the sound generated at frequencies of interest). The details of the argument for neglecting the above terms are given at the end of section 2.3 on pages 190-191 and at the end of section 2.5 on page 195 of Majumdar & Peake (1998). This argument is based on the large blade number,  $B$ , approximation of Parry & Crighton (1989)

and Crighton & Parry (1991); these references show that the blade numbers envisaged for the CROR certainly fall within the range of validity of the large  $B$  approximation.

## 2.2. Distorted turbulence spectrum

We are now in a position to calculate the distorted turbulence spectrum, given the turbulence spectrum at upstream infinity. We will be concerned with the frequency domain velocity correlation

$$S_{ij}(\mathbf{x}, \omega) = \int_{-\infty}^{\infty} R_{ij}(\mathbf{x}, \tau) \exp(i\omega\tau) d\tau, \quad (2.7)$$

where

$$R_{ij}(\mathbf{x}, \tau) = \langle u_i(\mathbf{x}, t), u_j(\mathbf{x}, t + \tau) \rangle, \quad (2.8)$$

and  $\langle \cdot, \cdot \rangle$  denotes an ensemble average. In particular we will be interested in the relationship between  $S_{ij}(\mathbf{x}, \omega)$  and the far-upstream turbulence spectrum  $S_{ij}^{\infty}(\mathbf{k})$ . Several analytic models exist for this latter quantity.

The distorted unsteady velocity, integrated over all wavenumbers, from equations (2.1) and (2.2), is given by

$$u_i(\mathbf{x}, t) = \frac{1}{(2\pi)^3} \int_{\mathbb{R}^3} A_{ik}(\mathbf{x}, \mathbf{k}) \hat{u}_k^{\infty}(\mathbf{k}) \exp\{i[k_x(X(\mathbf{x}) - U_{\infty}t) + k_y Y(\mathbf{x}) + k_z Z(\mathbf{x})]\} d^3\mathbf{k} \quad (2.9)$$

real part understood. The Fourier coefficient type integral  $\hat{u}_k^{\infty}(\mathbf{k}) = \int_{\mathbb{R}^3} u_k^{\infty}(\mathbf{y}, t) e^{-i\mathbf{k}\cdot\mathbf{y}} d^3\mathbf{y}$  provides us with the amplitudes previously represented by the quantity  $\mathbf{a}$ . Note that the frequency of the distorted velocity for a particular wavenumber  $\mathbf{k}$  is  $\omega = k_x U_{\infty}$ . Substituting (2.9) into (2.8) we have

$$\begin{aligned} R_{ij}(\mathbf{x}, \tau) &= \frac{1}{(2\pi)^6} \int_{\mathbb{R}^3} \int_{\mathbb{R}^3} \int_{\mathbb{R}^3} A_{ik}(\mathbf{x}, \mathbf{k}) A_{jl}(\mathbf{x}, \mathbf{k}') \exp(-ik'_x U_{\infty} \tau) \\ &\quad \exp\{-i[(k_x - k'_x)(X(\mathbf{x}) - U_{\infty}t) + (k_y - k'_y)Y(\mathbf{x}) + (k_z - k'_z)Z(\mathbf{x})]\} \\ &\quad \left[ \int_{\mathbb{R}^3} \langle u_k^{\infty}(\mathbf{y}), u_l^{\infty}(\mathbf{y}') \rangle \exp(i\mathbf{k}\cdot\mathbf{y}) \exp(-i\mathbf{k}'\cdot\mathbf{y}') d^3\mathbf{y} \right] d^3\mathbf{k}' d^3\mathbf{y}' d^3\mathbf{k}, \end{aligned} \quad (2.10)$$

as the ensemble average, after introducing a complex conjugation of  $u_i$ , acts upon the  $\mathbf{u}^{\infty}$  terms only. We make the substitution  $\mathbf{y}' = \mathbf{y} + \boldsymbol{\eta}$ , and for simplicity will consider homogeneous isotropic turbulence far upstream, which implies the ensemble average is independent of  $\mathbf{y}$ , allowing us to complete the  $\mathbf{y}$ ,  $\mathbf{k}'$  and  $\boldsymbol{\eta}$  integrals. Finally, substituting back into (2.7) gives

$$S_{ij}(\mathbf{x}, \omega) = \frac{2\pi}{U_{\infty}} \int_{\mathbb{R}^2} A_{ik}(\mathbf{x}, \mathbf{k}) A_{jl}(\mathbf{x}, \mathbf{k}) S_{kl}^{\infty}(\mathbf{k}) dk_y dk_z, \quad (2.11)$$

where now  $k_x = \omega/U_{\infty}$  and  $S_{kl}^{\infty}$  is the frequency domain velocity correlation at upstream infinity.

Equation (2.11) is the key result relating the turbulence at the rotor face to the turbulence far upstream. In order to produce specific noise predictions, we require a model for the form of the upstream turbulence. Wilson *et al.* (1999) summarised many of the assumptions commonly used by acousticians about the form of atmospheric turbulence, and compared these to findings of atmospheric scientists. Wilson indicates that the von Kármán spectrum fits measured atmospheric spectrum well, see Figure 3 in Wilson *et al.* (1999), and thus the assumptions of homogeneity and isotropy are reasonable ones. In



what follows we therefore substitute the isotropic spectrum

$$S_{ij}^\infty(\mathbf{k}) = \frac{E(k)}{4\pi k^4} (k^2 \delta_{ij} - k_i k_j), \quad (2.12)$$

where the well-known von Kármán energy spectrum is

$$E(k) = \frac{55g_1 \overline{u_{\infty,1}^2} L^5 k^4}{9(g_2 + k^2 L^2)^{\frac{17}{6}}}, \quad (2.13)$$

with  $g_1 \approx 0.1957$  and  $g_2 \approx 0.5578$ . Here  $\overline{u_{\infty,1}^2}$  is the mean square speed of the axial component of turbulent velocity, and  $L$  is the integral lengthscale. This is one of the most commonly used spectra (e.g. Lloyd (2009), Blandeau (2011)), and its use here allows ready comparison with other models. The integral lengthscale,  $L$ , is often taken by acousticians to be around 1 metre, but this is quite different to many observed measurements in the atmosphere, which often find  $L$  to vary proportionally to height off the ground Wilson *et al.* (1999); Wilson & Thomson (1994). In the current paper we will present results for a range of different  $L$  values.

### 3. Asymmetric mean flow models

In order to calculate a fully asymmetric turbulence spectrum (2.11) we next require appropriate asymmetric models for the mean flow  $\mathbf{U}$ , which determines the quantities  $\mathbf{X}$ . In this paper we consider two flows which model (i) the effect of an adjacent rotor or fuselage and (ii) flight incidence. For simplicity we use the well-known actuator disk (Hough & Ordway 1965), which captures the prominent features of streamtube contraction, to represent the rotor. Results for the turbulence spectrum at the rotor face are given in both cases. Further developments to account for other aspects of modern open rotor design, such as more general spanwise blade lift distributions and the effects of the nose bullet in static tests, will be given in a further publication (see also Robison (2011)).

#### 3.1. Asymmetric flow 1: adjacent rotors

The first asymmetric system we consider is shown in Figure 3(b), and consists of two actuator disks of radius  $r_d$  which lie in the  $y - z$  plane, separated by a distance  $d$  in the direction perpendicular to their axes. The mean flow is therefore given by the sum of two actuator disk flows, centred at  $(0, 0, 0)$  and  $(0, d, 0)$ . The strength of an actuator disk is defined to be  $U_d = T/\pi r_d^2 \rho_0 U_\infty$ , where  $T$  is the total propeller thrust and  $\rho_0$  is the mean fluid density - note that only the direction of thrust, and not the direction of rotation, appears in the actuator disk model. The axial and radial components of the mean flow generated by a single actuator disk are given in Appendix A of Majumdar & Peake (1998). The disk strength  $U_d$  determines the axial velocity at the fan face,  $U_f$ , and Hough & Ordway (1965) show that for a single disk in isolation  $U_f = U_\infty + U_d/2$ .

If the properties of both actuator disks are the same (strength  $U_d$ , and radius  $r_d$ ), then by symmetry we have zero normal velocity on the plane  $y = d/2$ , and the flow is equivalent to that of a single actuator disk at the origin next to an infinite rigid plane wall at  $y = d/2$ . This flow can therefore be used to approximately represent the effects of the presence of the fuselage on the distortion into a single open rotor. Note, however, that we will not be considering the subsequent scattering of the UDN by the fuselage; this issue has been considered by Kingan & McAlpine (2010), who calculated the acoustic Green's function in the presence of an infinite cylinder.

Sample results for the steady flow are given in Figure 3(a) in a high distortion case

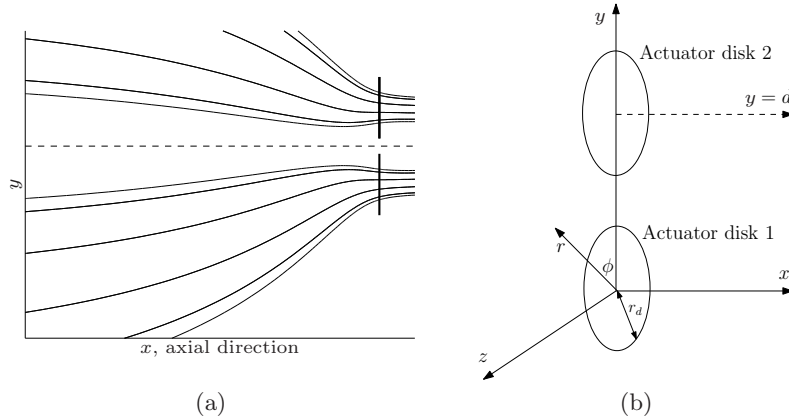


Figure 3: Illustration of asymmetric flow 1 which consists of two identical actuator disks side by side. (a) Streamlines for the two-disk system, for the high distortion case where  $U_f/U_\infty = 100$  for each rotor in isolation, with rotor separation  $d = 2.5r_d$ . The disk positions and line of symmetry are indicated by solid and dashed lines respectively. (b) Coordinate system used.

reminiscent of a static ground test. A crucial point to note here is that the streamlines arriving at a given radius on one actuator disk are strongly asymmetric, and the distortion experienced by the turbulence arriving at a given rotor radius will vary around the rotor. This becomes clear in Figure 4, where we have plotted the axial component of the distorted turbulence spectrum,  $S_{xx}$ , at a range of azimuthal positions around the disk. The overall spectral level increases as we move round from  $\phi = 0$ , the point nearest the second rotor, to  $\phi = \pi$ , the point furthest from the second rotor. As is clear in Figure 3 (a), the largest streamtube contraction occurs on the outboard section of the rotor, while the steady flow reaching the inboard section is closer to being axial (and uniform). This agrees with the notion that the flow contraction increases the level of axial coherence by stretching the inbound turbulent eddies.

We have also verified (not shown here) that when the value of separation  $d$  is increased the azimuthal variation of  $S_{xx}$  becomes much less pronounced, and the axisymmetric result is recovered. We have also observed (again not shown here) that the spectral level is greater at the blade tip than at the hub in all circumstances, due to the sharp velocity gradients at the edge of an actuator disk.

### 3.2. Asymmetric flow 2: rotor at incidence

Our second asymmetric mean flow models an open rotor at non-zero incidence angle,  $\alpha$ , to the flight direction, see Figure 5. In order to do this we follow Hanson (1995) and introduce tilted coordinates (denoted by primes), aligned with the actuator disk and related to the flight-direction coordinates via

$$x' = x \cos \alpha - z \sin \alpha, \quad y' = y, \quad z' = x \sin \alpha + z \cos \alpha, \quad (3.1)$$

with corresponding titled polar coordinates  $r'$  and  $\phi'$ . (Note that the directions of both the positive  $x$  and  $x'$  axes have been reversed compared to Hanson's coordinates.)

We construct the new flow by superposing an actuator disk flow in the  $\mathbf{x}'$  coordinate system on top of the flight mean flow  $U_\infty \hat{\mathbf{e}}_{\mathbf{x}}$ . As  $x' \rightarrow -\infty$  the  $\hat{\mathbf{e}}_{\mathbf{x}'}$  component of the mean flow tends to  $U_\infty \cos \alpha$ , and we neglect the cross-wind component of the flight speed,



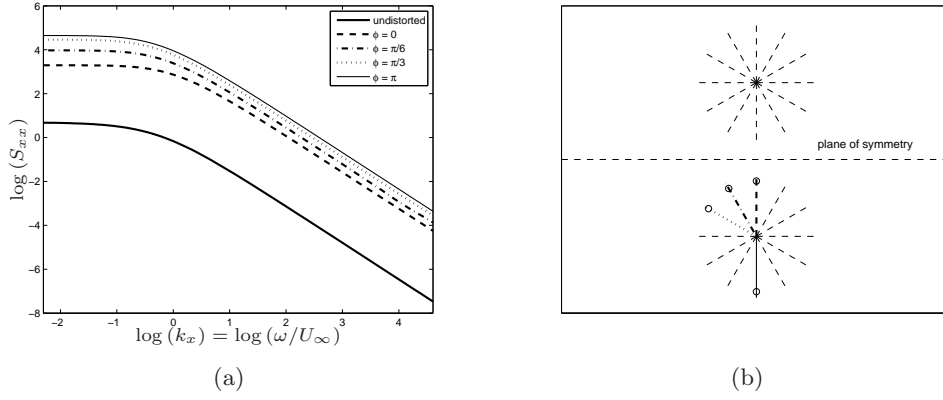


Figure 4: (a) Here we have calculated  $S_{xx}$  in a high distortion case ( $U_f/U_\infty = 100$ ) near the rotor tip ( $r = 0.9r_d$ ), at a range of azimuthal positions. For values of  $\phi$  between  $\pi/3$  and  $\pi$  the spectra become very close together. (b) This subfigure shows the azimuthal positions at which  $S_{xx}$  has been calculated. The open circles correspond to positions  $r = 0.9r_d$ . The value  $L = 0.5r_d$  has been used.

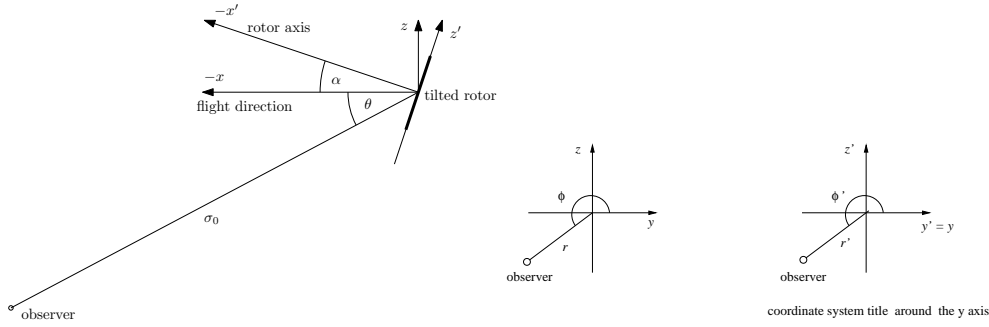


Figure 5: Coordinate system for rotor at incidence, both side on and head on views. The angle between the flight direction and the vector between the rotor origin and the observer is denoted by  $\theta$ . We denote the angle between the rotor axis and the vector between the rotor origin and the observer by  $\theta'$ . Note that  $\theta' \neq \theta + \alpha$  in general, equality is only satisfied when  $\phi = \pi/2$  or  $3\pi/2$ .

$U_\infty \sin \alpha \hat{e}_{z'}$ , in constructing the actuator disk flow. This approximation will be valid when  $\alpha$  is sufficiently small, or when the strength of the actuator disk is sufficiently large. For an open rotor in the pusher configuration,  $|\alpha|$  is typically less than  $3^\circ$  ( $\pi/60$  rad), and negative values of  $\alpha$  can occur during approach, whereas in the puller configuration  $|\alpha|$  is of the order of at most  $15^\circ$  ( $\pi/12$  rad). We therefore believe that the small-angle approximation is a reasonable one. The mean flow can now easily be calculated using the standard actuator disk velocities in the tilted coordinate system, with the 'effective' actuator disk strength at incidence being given by

$$U'_d = \frac{T}{\pi r_d^2 \rho_0 (U_\infty \cos \alpha)}. \quad (3.2)$$

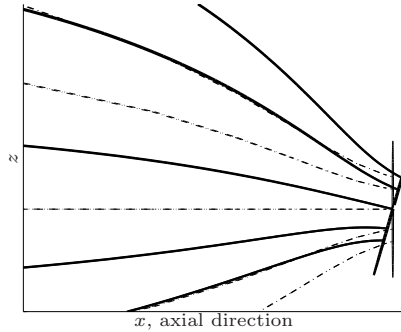


Figure 6: The streamlines induced by the actuator disk at incidence (solid), with the equivalent axisymmetric streamlines (dashed). The position of the disk in each case is also shown. Here  $\alpha = \pi/12$  rad and the total thrust,  $T$ , is kept constant between the two cases, with  $U_f/U_\infty = 100$  in the zero incidence case.

Figure 6 shows some representative plots of the streamlines for this tilted actuator disk set-up.

In Figure 7 we plot  $S_{xx}$  as the incidence angle  $\alpha$  is increased, at  $\phi' = \pi/2$  and  $\phi' = 3\pi/2$  which correspond to the points at the top and bottom of the actuator disk relative to the flight stream respectively. As  $\alpha$  increases the difference between the spectra at these two values of  $\phi'$  increases at first, but after a certain point decreases. This is explained by noting that if the tilted radial position of interest  $r'$  is kept constant, and  $\alpha$  is increased, then the non-tilted radial coordinate  $r$  at the two points ( $\phi' = \pi/2$  and  $3\pi/2$ ) gets closer to zero. That is, because

$$r = r' \cos \alpha \quad \text{for} \quad \phi' = \frac{\pi}{2} \quad \text{and} \quad \phi' = \frac{3\pi}{2}, \quad (3.3)$$

(see Figure 5) then as  $\alpha$  increases from zero,  $r$  decreases. Beyond a certain value of  $\alpha$  the fact that the streamlines arriving close to the centre of the disk experience a similar distortion in the journey from far upstream begins to counteract the difference introduced by the increased asymmetry.

#### 4. Blade unsteady pressure distribution

We next calculate the unsteady blade pressures induced when the distorted turbulence hits the rotor blades in the two cases. Specifically, we will decompose the incident turbulence into individual sinusoidal disturbances, and use a well-known cascade model to find the resulting blade response. The response from all the rotor blades, summed over all the individual incident disturbances, will then be used in §5 as the forcing term in the wave equation in order to obtain the far-field noise.

##### 4.1. Blade response theory

Smith (1973) analysed the response of a rectilinear cascade of idealised flat plate blades to an incident velocity perturbation, and Whitehead (1987) created the LINearized SUB-subsonic (LINSUB) code to implement Smith's theory. Within this framework, certain modelling assumptions apply. First, radial gradients are neglected, by 'unwrapping' the blade row and considering two-dimensional radial stations separately. This approximation allows the so-called cascade effects, the aerodynamic interaction between adjacent

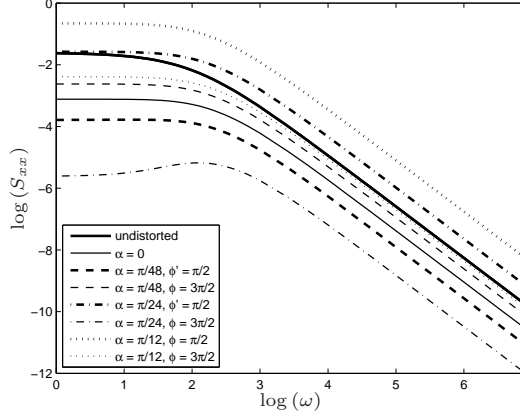


Figure 7: Plot of the axial component of the distorted turbulence spectrum as the angle of rotor incidence is varied. Here the distortion ratio is  $U_f/U_\infty = 10$ , and the spectrum is calculated at radial position  $r' = 0.4r_d$ , and axial position  $x' = -0.005r_d$ . The value of  $L = 0.5r_d$  has been used.

blades, to be taken into account. For an open rotor with perhaps 8 blades, cascade effects will not be as strong as for a conventional turbofan with perhaps 25 blades, but may become important near the rotor hub where the blades are more closely spaced. Second, the mean flow through the blade row itself is assumed to be uniform and aligned parallel to the blade chords. At each radial station the blades are then modelled as a chordwise distribution of spanwise line vortices whose strength is calculated so as to enforce the required condition of zero unsteady normal velocity on the blade surfaces.

Our unsteady input velocity into LINSUB takes the form of a convected sinusoidal gust, with the normal velocity at a particular blade leading edge having a given complex amplitude, and with the so-called inter-blade phase angle giving the phase difference between the velocities on adjacent leading edges. As shown in (2.9), the incident distorted turbulence may be described by an integration over wave vector  $\mathbf{k}$  of individual distorted gust components, weighted by the appropriate amplitude present in the turbulence far upstream. The blade normal velocity of these distorted components at a given blade leading edge for each upstream velocity component  $\hat{u}_j^\infty(\mathbf{k})$  is of the form

$$\hat{u}_j^\infty(\mathbf{k}) N_i(\mathbf{x}) A_{ij}(\mathbf{x}; \mathbf{k}) \exp\{i[k_x X + k_y Y + k_z Z]\} e^{-ik_x U_\infty t}, \quad (4.1)$$

where  $\mathbf{N}(r, \phi) = \sin \beta(r) \hat{\mathbf{e}}_x + \cos \beta(r) \hat{\mathbf{e}}_\phi$  is the blade normal vector and  $\beta$  is the angle of the blade to the axial direction. As described above, the blades are assumed to be aligned parallel to the local absolute mean flow velocity. For a rotor perpendicular to the flight direction (as in asymmetric flow 1) we therefore have  $\tan \beta(r) = \Omega r / (U_\infty + U_d/2)$ , and for a rotor at incidence (asymmetric flow 2) we have  $\tan \beta(r') = \Omega r' / (U_\infty \cos \alpha + U_d'/2)$ .

In order to calculate the blade response using LINSUB, we require the blade normal velocity (4.1) in a reference frame which rotates with the blades, decomposed into azimuthal harmonics. The method for doing this is described in the next two paragraphs, and we first use the formula (equation 8.511.4 on page 973 of Gradshteyn & Ryzhik

(1980))

$$\exp \{i [k_y \cos \Phi + k_z \sin \Phi] R\} = \sum_{n=-\infty}^{\infty} J_n \left( \sqrt{k_y^2 + k_z^2} R \right) \exp \left\{ in \left( \Phi - \phi_k + \frac{\pi}{2} \right) \right\} \quad (4.2)$$

to write

$$\begin{aligned} N_i A_{ij} \exp \{i [k_x X + k_y Y + k_z Z]\} &= \exp (ik_x X) [\sin \beta A_{xj} + \cos \beta A_{\phi j}] \\ &\times \sum_{n=-\infty}^{\infty} J_n (r_k R) \exp \left\{ in \left( \Phi - \phi_k + \frac{\pi}{2} \right) \right\}, \end{aligned} \quad (4.3)$$

recalling that  $Y = R \cos \Phi$  and  $Z = R \sin \Phi$ . Now, to bring out the  $\phi$  dependence in equation (4.3) explicitly in exponential form, we define a new Fourier coefficient quantity  $C_{ij}^{m,n}$  via

$$e^{ik_x X} A_{ij} (x, r; \mathbf{k}) J_n (r_k R) e^{in\Phi} = \sum_{m=-\infty}^{\infty} C_{ij}^{m,n} (x, r; \mathbf{k}) e^{im\phi}, \quad (4.4)$$

so that

$$C_{ij}^{m,n} (x, r; \mathbf{k}) = \frac{1}{2\pi} \int_0^{2\pi} e^{ik_x X} A_{ij} (x, r; \mathbf{k}) J_n (r_k R) e^{in\Phi} e^{-im\phi} d\phi. \quad (4.5)$$

Finally, we define quantities  $D_j^{m,n} \equiv N_i C_{ij}^{m,n}$ . Crucially, we require the quantities  $D_j^{m,n}$  in cartesian form, (i.e. for  $j = x, y, z$ ) in order to contract with  $\hat{u}_j^\infty$ , whereas  $N_i$  is most straightforwardly given in polar coordinates. Thus we convert from polar expressions for  $C_{ij}^{m,n}$  to ‘mixed suffices’ expressions, such as  $C_{\phi y}^{m,n}$ . Full details for the expressions for  $D_j^{m,n}$  are given in Appendix C.

For each wavevector  $\mathbf{k}$  the leading edge velocity in the direction normal to the blade can now be written in the form

$$\sum_{m=-\infty}^{\infty} w_W^m (x, r) e^{i\omega_\Gamma t + im\hat{\phi}}, \quad (4.6)$$

where  $\hat{\phi} = \phi - \Omega t$  is the azimuthal coordinate in the rotating frame,  $\omega_\Gamma = m\Omega - k_x U_\infty$  are the harmonics of the gust frequency in the rotating frame, and the modal coefficients  $w_W^m$  are given by

$$\begin{aligned} w_W^m e^{i\omega_\Gamma t + im\hat{\phi}} &= \sum_{n=-\infty}^{\infty} D_j^{m,n} (x_0(r), r; k_x, r_k, 0) \exp [-i(m+n)\phi_k] e^{-\frac{in\pi}{2}} \\ &\hat{u}_j^\infty (\mathbf{k}) \exp [i(m\Omega - k_x U_\infty) t] \exp [im\hat{\phi}]. \end{aligned} \quad (4.7)$$

The  $\exp(-im\phi_k)$  factor here has arisen from the expression for  $D_j^{m,n}$  when the argument  $\phi_k$  is set to zero (see equation (C3)). For each term in (4.6) it follows straight away that the interblade phase angle (which gives the phase difference occurring between adjacent blades) is  $-\frac{2\pi m}{B}$ , where  $B$  is the number of rotor blades. The minus sign occurs because we are using the *direct* reference frame, where  $\phi$  runs anticlockwise when the axial direction is out of the page, see Figure 5.

The pressure jump can now be calculated using LINSUB, and the pressure jump across a blade which passes through the position  $(x, r, \phi)$  at time  $t$ , due to an upstream gust of

the form  $\hat{\mathbf{u}}^\infty(\mathbf{k})e^{i(\mathbf{k}\cdot[\mathbf{x}-U_\infty t\hat{\mathbf{e}}_x])}$  is finally given by

$$\Delta p(x, r, \phi, t) = \rho_0 W \sum_{m=-\infty}^{\infty} \gamma^m \left\{ \sum_{n=-\infty}^{\infty} D_j^{m,n}(x_0(r), r; k_x, r_k, 0) e^{-i(m+n)\phi_k} e^{-\frac{in\pi}{2}} \right\} \hat{u}_j^\infty(\mathbf{k}) e^{-ik_x U_\infty t} e^{im\phi}. \quad (4.8)$$

The various terms in (4.8) are explained as follows: the factor  $\rho_0 W$  is included to give the dimensional pressure jump, where  $\rho_0$  is the mean density and  $W$  is the absolute mean flow velocity in the rotating frame at each radius;  $\gamma^m$  is the bound vorticity distribution on the blade resulting from the gust interaction, and is an output from LINSUB (see Whitehead (1987) for the full details); and the remaining terms in (4.8) come from the individual gust amplitudes. The arguments of the bound vorticity are  $\gamma^m = \gamma^m(x, r, \omega_\Gamma)$ , with  $x, r$  being the position of a given point on the blade and where we recall that  $\omega_\Gamma$  is the gust frequency in the rotating frame. In the non-zero incidence case, asymmetric flow 2 in the present paper, the quantities  $x, r$  (and  $\phi$  in earlier equations) are replaced by their primed equivalents.

#### 4.2. Limits on the radial wavenumber

As we have already noted, Smith's two-dimensional blade response model neglects radial gradients, i.e. for an input gust of the form  $e^{ik_s r + im\phi}$  the  $e^{ik_s r}$  factor is taken as part of the amplitude of the incident gust at each  $r$  station. Formally, there is therefore no limit to the value of  $k_s$  which could be used in the blade response. However, the sound waves which we will ultimately obtain from solving the wave equation with these blade forces will satisfy the Helmholtz equation, and this will necessarily limit the range of values of  $k_s$  which can eventually contribute to the radiated sound. We expect that, while all radial wavenumbers in the blade forcing generate near-field pressure perturbations, it will only be values of  $k_s$  in a finite range which lead to propagating acoustic waves and therefore contribute to the far-field sound. However, the expression for the incident velocity field, as given in equation (4.7), does not have  $r$  dependence written explicitly in the form  $e^{ik_s r}$ , and we therefore need to determine an expression for the 'effective' radial wavenumber (equivalent to  $k_s$ ) when we have a general  $r$  dependence within the velocity input, e.g. denoted by  $f(r)$ .

The situation is not completely straightforward, as we wish to translate between the full cylindrical geometry in which the incident turbulence is distorted and the sound is radiated and the rectilinear geometry in which the blade response is computed. This is a well-known difficulty in turbomachinery noise studies, and Posson *et al.* (2010) and Glegg & Jochault (1998) have looked at the problem of translating between these two coordinate systems in a similar context. Posson *et al.* (2010) noted that, in addition to the wave equation being satisfied in each of the two geometries, there are (at least) two conditions which one would ideally like to satisfy when moving between the cylindrical and rectilinear geometries: first, keeping the magnitude and direction of the wavevector components in a plane of constant radius the same between the two geometries; and second, matching the spanwise and radial structures, for instance by decomposing the cylindrical Bessel functions into exponentials, from which the  $k_s$  can easily be read off. However, they showed it was not possible to satisfy both of these conditions at once, and in what follows we choose to satisfy the first of these conditions only.

We identify  $r$  in the cylindrical geometry with the spanwise rectilinear coordinate in the cascade geometry and  $-r\phi$  with the transverse coordinate (again, the minus sign being

due to use of the direct reference frame). Given a disturbance of the form  $f(r)e^{i\omega t+im\phi}$ , as was obtained by rewriting  $\mathbf{u}$  in the form of equation (4.6), we wish to equate this to a wave in the rectilinear geometry. Identifying the wavevector in a plane of constant radius in the two geometries, we can straightforwardly identify the transverse wavevector  $k_t$  with  $-m/r$ . In order for the disturbance to satisfy the wave equation in both geometries, given that the time dependence is fixed, we also equate the result of applying the  $\nabla^2$  operator, to find

$$k_s^2 + k_t^2 = -\frac{\frac{1}{r}\frac{\partial}{\partial r}\left(r\frac{\partial f}{\partial r}\right)}{f(r)} + \frac{m^2}{r^2} \quad (4.9)$$

which implies that

$$k_s^2 = -\frac{\frac{1}{r}\frac{\partial}{\partial r}\left(r\frac{\partial f}{\partial r}\right)}{f(r)}. \quad (4.10)$$

This gives a general formula for picking out the effective radial wavenumber from an expression with general  $r$  dependence. In our case the primary  $r$  dependence within our velocity expression (4.3) takes the form  $J_n(r_k R)$ , (as Cargill (1993) did, we neglect the  $r$  dependence within  $e^{ik_x X}$  and  $e^{in\Phi}$  in determining  $k_s$ ) and thus we find

$$k_s^2 = r_k^2 \left(\frac{\partial R}{\partial r}\right)^2 \left(1 - \frac{n^2}{r_k^2 R^2}\right) - \left(\frac{r_k}{r}\frac{\partial R}{\partial r} + \frac{r_k}{r}\frac{\partial^2 R}{\partial r^2} - \frac{r_k}{R}\left(\frac{\partial R}{\partial r}\right)^2\right) \frac{J'_n(r_k R)}{J_n(r_k R)}. \quad (4.11)$$

It turns out that  $R$  is very close to being a linear function of  $r$  for the actuator disk model of distortion we employ, except near the blade tip, so that in practice the second set of terms in (4.11) are negligible (they would be identically zero for an exactly linear  $R$ ). This leads to the relation

$$r_k^2 = \frac{k_s^2}{\left(\frac{\partial R}{\partial r}\right)^2} + \frac{n^2}{R^2}. \quad (4.12)$$

It is certainly the case that  $0 \leq k_s^2 \leq \omega^2/c_0^2$  (with the upper limit coming from the frequency term in the Helmholtz equation,  $c_0$  being the speed of sound), and we can use this to impose finite limits in the  $r_k$  integrals found when solving for the far-field pressure. We therefore impose

$$\sqrt{\frac{n^2}{R^2}} \leq r_k \leq \sqrt{\left(\frac{\partial R}{\partial r}\right)^{-2} \frac{\omega^2}{c_0^2} + \frac{n^2}{R^2}}. \quad (4.13)$$

Since  $n$  and  $r_k R$  are respectively the order and argument of the Bessel function which governs the radiation, the lower limit here is a statement that it is only when the argument of the Bessel function is greater than its order that the source radiates, as previously noted by Parry (1988). Within the upper limit, the quantity  $\partial R/\partial r$  expresses the effect of the streamtube contraction;  $\partial R/\partial r$  increases from a value of unity far upstream as we move towards the rotor. In analogy to sound propagating in a contracting duct, we can therefore interpret the quantity

$$\left(\frac{\partial R}{\partial r}\right)^{-1} \frac{\omega}{c_0} \quad (4.14)$$

as being proportional to an effective Helmholtz number, which controls which parts of the acoustic field can propagate to the far field. Having now introduced finite limits on the radial wavenumber, we are in a position to compute the far-field radiation.

As a final point in this section, we wish to emphasise that unwrapping the rotor in

cylindrical geometry into a cascade in cartesian geometry is obviously an approximation, but one which is necessary given that a computational solution to our problem with a full incident turbulence spectrum and full annular geometry is some way off. The accuracy of the cascade approximation has recently been investigated by Posson *et al.* (2013), who compared cascade responses with a fully numerical annular solution in the case of a single incident sound wave and a ducted rotor. They found that the cascade model can give reasonable results, but that significant errors can occur in individual cases, typically at combinations of frequencies and wavenumbers when duct modes are close to cut-off. Posson *et al.* (2013) are able to produce better results in such cases by matching the wavenumbers between annular and planar geometries, which is precisely how we limited the integration over radial wavenumbers in this subsection. The accuracy of the cascade approximation remains an open question, but it seems reasonable to expect that the combination of averaging over a broadband input forcing and correction of the limits of integration over radial wavenumbers serves to reduce the errors in our particular problem.

## 5. Far-field noise

The unsteady blade lift distribution generated by the interaction of the rotor with the distorted turbulence was calculated in the previous section, and we now compute the far-field sound generated by this unsteady force distribution. The sound generation is described by the convected wave equation (Dowling & Ffowcs Williams 1983)

$$\nabla^2 p - \frac{1}{c_0^2} \left( \frac{\partial}{\partial t} + U_\infty \frac{\partial}{\partial x} \right)^2 p = \nabla \cdot \mathbf{f}(\mathbf{x}, t) \equiv - \int_\omega Q_\omega(x, y, z) e^{-i\omega t} d\omega, \quad (5.1)$$

where  $p$  is the fluid pressure and  $\mathbf{f}$  is the force per unit volume applied to the fluid (in this case by the rotor blades), which can be described as an integral of sources  $Q_\omega$  over a continuous frequency spectrum for broadband noise (or a sum of discrete frequencies for purely tonal noise). In this section we will first describe the expression found for  $\mathbf{f}$  in our asymmetric set-up, and then the Green's function solution to the above equation.

### 5.1. Forcing term

To obtain  $\mathbf{f}$  we multiply each blade pressure jump as given in equation (4.8) by a delta function corresponding to the location of blade  $b$  at time  $t$

$$\delta \left[ r \left( \phi - \Omega t - \phi_0(r) - \frac{2b\pi}{B} \right) - (x - x_0(r)) \tan \beta(r) \right], \quad (5.2)$$

where  $x_0, \phi_0$  give the leading edge of the blade at time  $t = 0$ . We then sum over all blades,  $b$  running from 1 to  $B$ , and re-express that delta function series as a sum (over the new index  $l$ ) of complex exponential terms. We find

$$\begin{aligned} f_i(x, r, \phi, t) &= \rho_0 W N_i(r) \frac{B}{2\pi r} \sum_{m=-\infty}^{\infty} \frac{1}{(2\pi)^3} \int_{\mathbb{R}^3} \gamma^m(x, r; k_x) \exp(-ik_x U_\infty t) \\ &\quad \sum_{n=-\infty}^{\infty} D_j^{m,n}(r; k_x, r_k) e^{-i(m+n)\phi_k} \left[ \int_{\mathbb{R}^3} u_j^\infty(\mathbf{x}') e^{-i\mathbf{k} \cdot \mathbf{x}'} d^3 \mathbf{x}' \right] d^3 \mathbf{k} \\ &\quad \sum_{l=-\infty}^{\infty} \exp \left( i(m+lB) \left[ \frac{(x - x_0(r)) \tan \beta(r)}{r} \right] \right) \exp(-ilB\phi_0(r)) \\ &\quad \exp(-ilB\Omega t) \exp(i[m+lB]\phi). \end{aligned} \quad (5.3)$$



Here we see that azimuthal dependence has been explicitly separated out. For each  $k_x$  we can define components  $F^{m,n,l}$  so that

$$\mathbf{f} \equiv \mathbf{N} \sum_{m,n,l} F^{m,n,l}(x, r; k_x) e^{-i(k_x U_\infty + lB\Omega)t} e^{i[m+lB]\phi}. \quad (5.4)$$

Defining  $\omega = k_x U_\infty + lB\Omega$  we then find

$$Q_\omega(x, y, z) = - \sum_{m,n,l} \left[ \sin \beta(r) \frac{\partial F^{m,n,l}}{\partial x} + \frac{\cos \beta(r)}{r} i(m+lB) F^{m,n,l} \right] e^{i[m+lB]\phi}, \quad (5.5)$$

where the integration variable in equation (5.1) will now be  $k_x$ . In the non-zero incidence case the quantities  $x, r$  and  $\phi$  in (5.5) are replaced by their primed equivalents.

### 5.2. Green's function for rotor at incidence

The solution to equation (5.1) can be written in the form

$$p(x, y, z, t) = \int_\omega P_\omega(x, y, z) e^{-i\omega t} d\omega. \quad (5.6)$$

The Green's function for a rotor travelling at some non-zero angle of attack to its axis was calculated by Hanson (1995), noting that the opposite sign convention for the positive  $x$  axis was used in that paper. In the tilted system, Hanson finds the solution of equation (5.1) to be

$$P_\omega(\sigma_0, \theta', \phi') = \frac{e^{\frac{i\omega\sigma_0}{c_0}}}{4\pi\sigma_0(1-M\cos\theta)} \int_{r'_s=0}^{r_d} \int_{x'_s=-\infty}^{\infty} \int_{\phi'_s=-\pi}^{\pi} Q_\omega(x'_s, r'_s, \phi'_s) \exp \left[ \frac{-i\omega}{c_0(1-M\cos\theta)} (x'_s \cos \theta' + r'_s \sin \theta' \cos(\phi' - \phi'_s)) \right] r'_s d\phi'_s dx'_s dr'_s, \quad (5.7)$$

where we integrate over the source coordinates  $(x'_s, r'_s, \phi'_s)$ . We can express  $\cos \theta$ , which appears in two places, in terms of primed coordinates as

$$\cos \theta = \cos \theta' \cos \alpha - \sin \theta' \sin \phi' \sin \alpha. \quad (5.8)$$

The changes from the standard (non-tilted) Green's function are only in the phase term; in the far-field, the amplitude terms are the same to leading order. The solution in the non-tilted case (used for our asymmetric flow 1) is therefore identical to (5.7) except  $\theta'$  and  $\phi'$  are replaced by  $\theta$  and  $\phi$  everywhere.

For sources with azimuthal dependence of the form  $e^{iq\phi}$ , as we have, the  $\phi'_s$  integral in (5.7) can be done explicitly, yielding a Bessel function, and a final manipulation involves integrating the first term from equation (5.5) by parts.

We take the auto-correlation of  $p$  and then take the Fourier Transform to find the Power Spectral Density (PSD),  $\hat{P}(\mathbf{x}, \omega)$ , as follows

$$\begin{aligned} \hat{P}(\mathbf{x}, \omega) &= \int_{-\infty}^{\infty} \langle (p(\sigma_0, \theta, \phi, t)), p(\sigma_0, \theta, \phi, t + \tau) \rangle e^{i\omega\tau} d\tau \\ &= \int_{-\infty}^{\infty} P(\sigma_0, \theta, \phi, \tau) e^{i\omega\tau} d\tau. \end{aligned} \quad (5.9)$$

Majumdar (1996) then integrated  $\hat{P}$  over a shell of radius  $\sigma_0$  in the far-field, removing  $\phi$  and  $\sigma_0$  dependence, to find

$$P(\omega) = \int_{\phi=0}^{2\pi} \int_{\theta=0}^{\pi} \hat{P}(\mathbf{x}, \omega) \sigma_0^2 \sin \theta d\theta d\phi, \quad (5.10)$$

In this paper we therefore plot the spectral power quantity

$$\Sigma(\omega) \equiv 10 \log_{10} \left( \frac{P(\omega)}{10^{-12}} \right) \text{dB}, \quad (5.11)$$

which gives the correct trends of location and relative heights of tones. These are the key results of this work, since the absolute levels are ultimately controlled by the magnitude of the upstream turbulence intensity,  $u_{\infty,1}^2$ .

The full expression obtained is rather cumbersome, and is given in full in Appendix D. Within the triple summation found in equation (D1), the  $n$  index arose from the Bessel function and upstream azimuthal angle dependence within the incident velocity,  $J_n(r_k R) e^{in\Phi}$ , and the  $m$  index corresponds to the total azimuthal order of the incident turbulence field upon the blades - see equation (4.4). The  $l$  index arose from the  $2\pi/B$  periodicity of the blades.

## 6. Radiated noise results

### 6.1. Asymmetric flow 1: adjacent rotors

In Figure 8 we plot the radiated sound  $\Sigma(\omega)$  from a single rotor of an adjacent rotor pair, with the asymmetrical inflow described in section 3.1, in cases of low, medium and high distortion. As expected, and as discussed in the introduction, strong narrow tones are generated at multiples of blade passing frequency in the high distortion (static) case, due to the stretching of eddies by the significant streamtube contraction. In contrast, in the low distortion (flight) case tones are not generated, because the weak streamtube contraction now has only a small effect on the axial coherence of the (broadband) incident turbulence, and a broadband noise spectrum is produced. Of course, the mid-level distortion case lies between these two extremes, but note that even here tones can be generated which protrude more than 20dB above the minimum broadband level. The absolute level of all three plots depends on the value assigned to  $u_{\infty,1}^2$ , which provides only a vertical shift to the spectra, and in each case here this has been set to the same value. In reality, the turbulence intensity will vary significantly between different aircraft operating conditions (with presumably very much lower levels at higher altitude in flight than at take-off). When comparing spectra for *different* distortion levels we therefore seek to compare only the spectral shapes, rather than the absolute levels.

In order to further investigate the effect of the streamtube contraction on the different parts of the spectrum, we plot in figure 9 the change in  $\Sigma(\omega)$  as the integral lengthscale is varied, here in the mid-level distortion case. For a typical broadband frequency, we see that the power level varies linearly on this logarithmic plot, with  $P(\omega)$  decreasing like  $L^{-2/3}$  across the whole range of integral length scales considered. This behaviour can be seen precisely in the energy spectrum of the undistorted turbulence far upstream; by keeping  $k$  fixed (equivalent to fixing  $\omega$  and taking  $k \sim \omega/U$ ) we see from (2.13) that  $E(k) \sim L^{-2/3}$  for  $L$  large. For the broadband component the behaviour of the acoustic energy therefore simply mirrors the behaviour of the turbulent energy spectrum far upstream. In contrast, at the tonal frequency the  $L^{-2/3}$  fall-off is modified, with a maximum power level observed for an integral lengthscale  $L$  comparable to the propeller radius. For large values of  $L$  the decay again matches the  $L^{-2/3}$  behaviour found for the broadband component. From this we can conclude that the effects of the distortion, at least in terms of modifying the energy distribution between the input turbulence upstream and the output far-field noise, are more significant for the tones than for the broadband.

In Figure 10 we compare spectra for three different values of the rotor spacing  $d$ ,

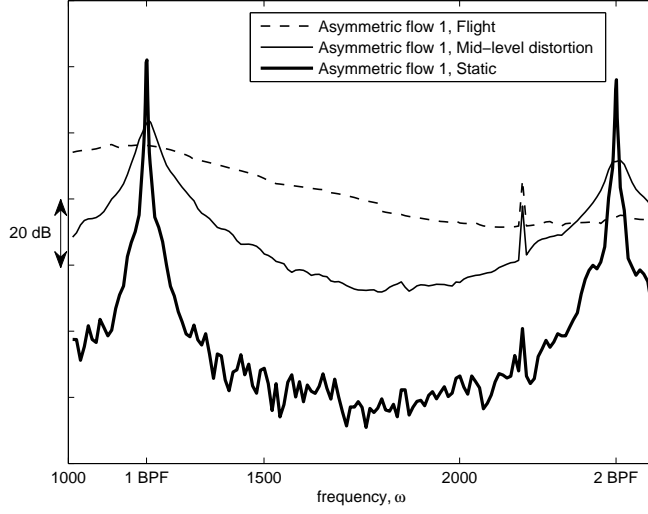


Figure 8: Plots of spectral power quantity  $\Sigma(\omega)$  from a single rotor in asymmetric inflow (as given by asymmetric flow 1, with  $d = 2.5r_d$ ) at three different distortion levels. The *Flight* condition corresponds to  $U_f/U_\infty = 1.18$ , *Mid-level distortion* to  $U_f/U_\infty = 10$ , and *Static* to  $U_f/U_\infty = 100$ . The integral lengthscale was taken to be  $L = 0.5r_d$ . In this figure, and throughout the rest of the paper, we take  $B = 12$  and  $\Omega = 100\text{rads}^{-1}$ .

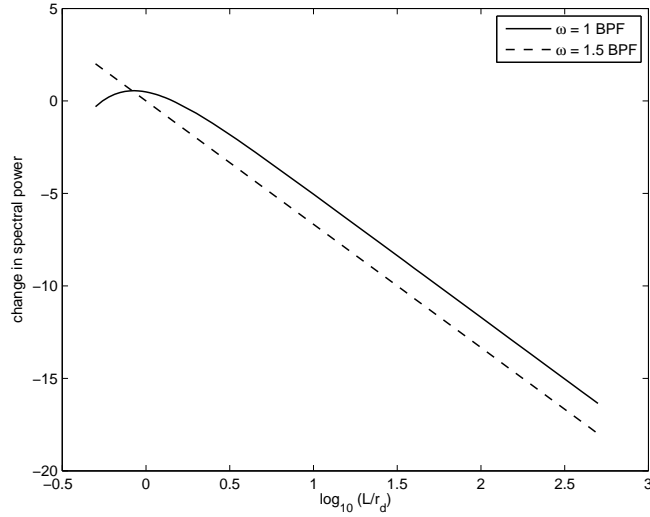


Figure 9: Effect of varying integral lengthscale  $L$  on  $\Sigma(\omega)$  at tonal ( $\omega = 1\text{BPF}$ ) and representative broadband ( $\omega = 1.5\text{BPF}$ ) frequencies, relative to the level for  $L = r_d$ . Here we have the mid-level distortion case.

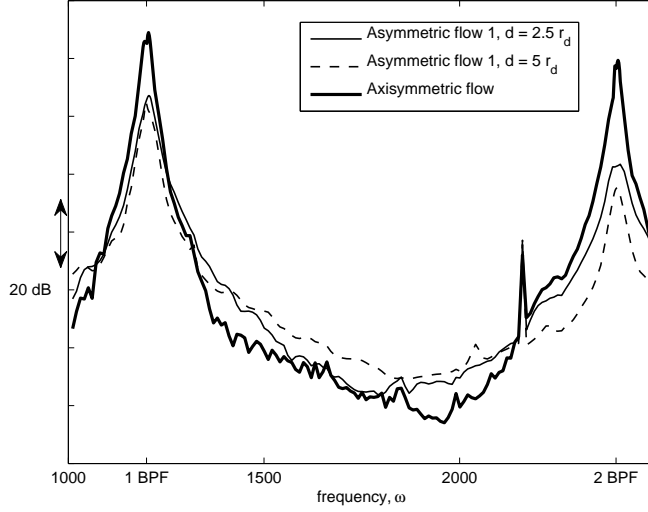


Figure 10: Plots of  $\Sigma(\omega)$  from a single rotor in asymmetric inflow (asymmetric flow 1) for varying the rotor spacing  $d$ , in the case of *Mid-level distortion*  $U_f/U_\infty = 10$  and other conditions as in figure 8.

in order to assess the effects of asymmetry. A very strong effect on the tonal levels is observed, with a significant increase at both one and two BPF, as  $d$  increases from the highly asymmetric case  $d = 2.5r_d$  (corresponding to a tip separation of just half of one radius) to axisymmetric case in which  $d$  is effectively infinite (in fact, for cases of  $d \geq 25r_d$ , the spectra produced are visually indistinguishable from the axisymmetric case). The reason for this behaviour, we believe, is that the close proximity of the second rotor forces the oncoming flow to remain more parallel in the region between the rotors, thereby reducing the effective streamtube contraction into the rotor compared to the (symmetric) isolated-rotor case. The effect of varying asymmetry on the broadband component is smaller, and less systematic, than in the tonal case, in agreement with the conclusion of the previous paragraph.

Note that in Figures 8 and 10 a smaller intermediate peak occurs in the mid-level distortion case, and is evident in the static case in Figure 8. We note that tones at non-multiples of BPF arise when the  $n$ th azimuthal order of a steady incident disturbance interacts with the rotor to generate sound of frequency  $(mB \pm n)\Omega$ ; the intermediate peak seen here occurs at  $\omega = (2B - 2)\Omega$ . Of course, the incident turbulence contains components at all frequencies and all azimuthal orders, and we hypothesise that one of these azimuthal-order interactions leads to the intermediate peak. However, the precise reason why this particular intermediate peak should be selected is not clear to us.

### 6.2. Asymmetric flow 2: rotor at incidence

The qualitative effects of increased levels of distortion on the character of the spectra are the same as shown in figure 8 for asymmetric flow 1, i.e. high distortion leads to the generation of strong peaks at multiples of BPF. In order to consider the quantitative effects of asymmetry, we plot in figure 11 the change in power level for increasing  $\alpha$  relative to the axisymmetric ( $\alpha = 0$ ) case. This is again for mid-level distortion, for the first two BPF tones and for the representative broadband frequency  $\omega = 1.5\text{BPF}$ .

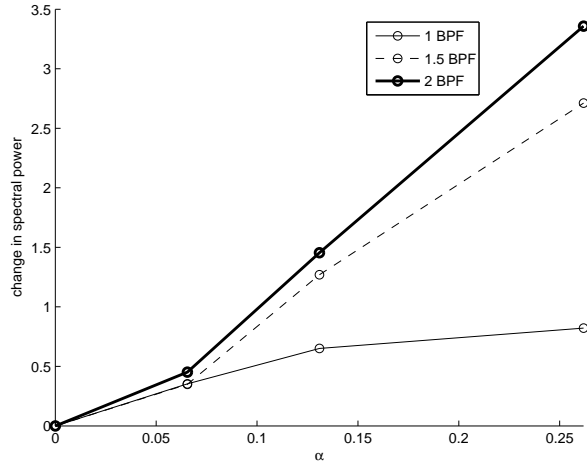


Figure 11: Effect of varying incidence angle  $\alpha$  (in radians) on  $\Sigma(\omega)$  at tonal ( $\omega = 1, 2\text{BPF}$ ) and representative broadband ( $\omega = 1.5\text{BPF}$ ) frequencies, relative to the level for  $\alpha = 0$ . Here we have the mid-level distortion case, and  $L = 1$ .

For all three frequencies the spectral power increases with  $\alpha$ , but only significantly for the broadband and the 2BPF frequencies, while the 1BPF tonal is relatively insensitive. No clear difference between the behaviour of the tonal and broadband levels therefore emerges, in the way that it did for the variation of integral length in figure 9 for asymmetric flow 1. However, this is perhaps not surprising for two reasons; first, there is no simple connection between the incidence angle and the level of distortion, as became clear in figure 7; and second, as  $\alpha$  changes the radiated power is affected not only by the flow distortion but also by the Hanson (1995) geometrical effect of tilting the plane of rotation of the acoustic sources. In this sense, the noise behaviour of asymmetric flow 2 is more complicated than that of asymmetric flow 1.

In order to assess the effects of incidence angle on the sound directivity, in figure 12 we consider the quantity

$$10 \log_{10} \left( \sigma_0^2 |\hat{P}(\mathbf{x}, \omega)| \right), \quad (6.1)$$

with  $\hat{P}(\mathbf{x}, \omega)$  given in (D 1). At the tonal frequency  $\omega = 1\text{BPF}$  we see that the directivity is very similar for observers directly above ( $\phi' = \pi/2$ ) and directly below ( $\phi' = 3\pi/2$ ) the rotor and for the two incidence angles considered, indicating that the asymmetry of the mean flow is having only a small effect. This agrees with figure 11, in which the integrated power level is seen to be rather insensitive to the incidence angle. In contrast, at the broadband frequency  $\omega = 1.5\text{BPF}$  the effect of incidence angle on the directivity as a function of  $\theta$  is much more significant (as it was in figure 11 for the integrated power level). Interestingly, however, the asymmetry of the directivity as  $\phi'$  varies is still very weak; in figure 12b, the directivities for  $\phi' = \pi/2, 3\pi/2$  are very similar indeed (and at the lower incidence angles are indistinguishable). The asymmetries in  $\phi'$  in the incident turbulence spectra which we observed in figure 7 have therefore not been translated into  $\phi'$  variations in the radiated field. It appears that the azimuthal variation in the radiation field which would presumably result from the interaction of the rotor with a single gust are averaged out when integrating over a full turbulence spectrum.

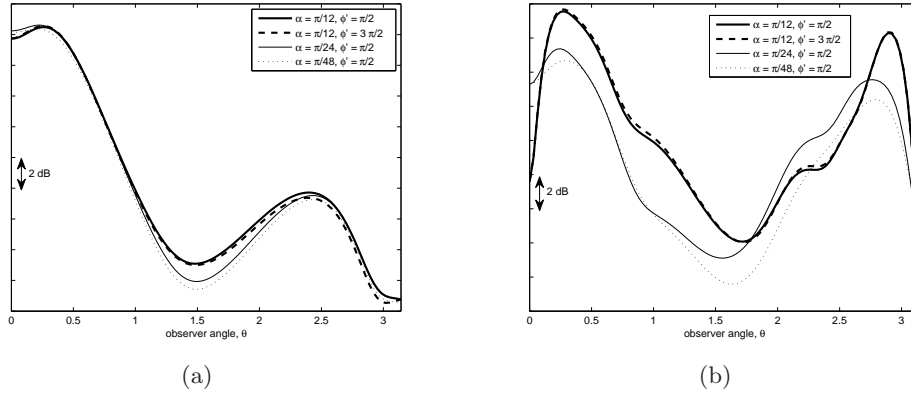


Figure 12: (a) Directivity patterns for a rotor at three different angles of incidence,  $\alpha = \pi/12, \pi/24$  and  $\pi/48$ , at the tonal frequency  $\omega = 1$  BPF. In the case of  $\alpha = \pi/12$  two different azimuthal positions are shown (for  $\alpha = \pi/12, \pi/24$  the directivities at different  $\phi'$  are indistinguishable) (b) Similarly, for broadband frequency  $\omega = 1.5$  BPF.

We note that the  $\theta$  directivity seen in figure 12 is characteristic of unsteady distortion noise, with higher amplitudes upstream and lower amplitudes in the plane of the rotor (directivity plots for asymmetric flow 1 are very similar). This is due to the predominance of Bessel functions of order zero in the expression for the acoustic pressure (see the discussion in Appendix D).

## 7. Concluding remarks

In this paper we have set out a method for predicting the generation of unsteady distortion noise by the ingestion of turbulence into a rotor, in situations in which the inflow is asymmetric, thereby extending the previous analysis of Majumdar & Peake (1998) who considered axisymmetric flow. We have specifically considered two cases of practical interest; adjacent twin rotors, and a single rotor at incidence. A key part of our work here has been the inclusion of the polar forms of the distorted wavenumber vector  $\mathbf{l}$  and distortion tensor  $\mathbf{A}$ ; in computing the results we found that inclusion of all the azimuthal terms described in this paper was required. Another key feature of the analysis is that it is essential to limit the integral over transverse wavenumber,  $r_k$ , in order to achieve convergence. This is due to our use, as is standard, of strip-theory models of the blade response, but this difficulty can be eliminated in the future, when computational resources allow, by the use of fully three-dimensional response models for annular blading.

We saw different types of behaviour in the two asymmetric flows. For adjacent rotors, we concluded that the level of mean-flow asymmetry, as measured by the proximity of the two rotors, significantly reduces the tonal levels compared to the axisymmetric case. In contrast, the effect of the distortion on the broadband noise seems less significant. For a rotor at incidence the picture is more complicated, due to the fact that changing the incidence angle not only changes the level of distortion but also changes the radiation properties of the rotor. However, what is certainly clear is that incidence can have a significant effect, with for instance a more than 3dB increase in the radiated power at the 2BPF tone when the incidence is increased from  $0^\circ$  to  $15^\circ$ .

A number of extensions of this work have been considered, including investigating the effect of using a Gaussian expression for the energy spectrum  $E(k)$  within the context of isotropic turbulence, more complicated models of the propeller lift distribution (as opposed to the simple uniform actuator disk theory used here), and the influence of the propeller mounting used in wind tunnel tests. These issues are discussed in Robison (2011). Directions for further work, suggested by an anonymous referee, are as follows. One would be to investigate differences that might be experienced between rotors in pusher and puller configurations. For instance, in the pusher configuration, when the rotor is mounted at the rear, the effect of the proximity of the fuselage might be better modelled by a semi-infinite plane, rather than the infinite plane used in our asymmetric flow case 1 here. A second suggested direction would be consideration of non-isotropic, inhomogeneous turbulence incident from upstream infinity. This is certainly possible within the RDT framework, but would obviously require the input turbulence to be specified in detail - one possibility might be to use experimentally-measured spectra, as is done by Alexander *et al.* (2013). A third possibility would be to investigate near-field noise levels, with a view to establishing how the near axisymmetry observed in the far-field directivity breaks down close to the rotor.

RAVR acknowledges funding from an EPSRC Rolls Royce CASE award which made this work possible. The authors are most grateful to Dr AB Parry for many helpful discussions.

## Appendix A. Polar representation of the wave vector $\mathbf{k}$

We require expressions for the component of the incident turbulent velocity in the direction of the blade surface normal,  $\mathbf{N}$ . Since  $\mathbf{N}$  has components in the axial and azimuthal directions - see equation (4.1) - it will be most convenient to translate various quantities into coordinates aligned with the vector  $\mathbf{x}$ , see Figure 13 where the different coordinate representations of  $\mathbf{x}$  and  $\mathbf{k}$  are illustrated. In physical space we write

$$\mathbf{X}(\mathbf{x}) = X\hat{\mathbf{e}}_x + R\cos(\Phi - \phi)\hat{\mathbf{e}}_r + R\sin(\Phi - \phi)\hat{\mathbf{e}}_\phi, \quad (\text{A } 1)$$

where  $R = \sqrt{Y^2 + Z^2}$  is the far-upstream value of  $r$  for the streamline running through the point  $\mathbf{x}$ , and  $\Phi = \tan^{-1}(Z/Y)$  is the far upstream azimuthal angle (recall that the mean flow is aligned with the polar axis far upstream). After some algebra, expressions for the three polar components of  $\mathbf{l}$  (e.g. the radial component  $l_r = \mathbf{l} \cdot \hat{\mathbf{e}}_r$ ) and the nine polar components of  $\mathbf{A}$  (e.g.  $A_{rr} = \hat{\mathbf{e}}_r \cdot \mathbf{A} \cdot \hat{\mathbf{e}}_r$ ) can be derived, and are given in Appendix B.

From Figure 13 we see that  $k_r$  and  $k_\phi$  give  $\mathbf{k}$  in a cartesian base which has been rotated to align with the vector  $\mathbf{x}$ . For subsequent numerical calculations it will also be helpful to re-express the wave vector  $\mathbf{k}$  in a polar form, which allows us to convert certain of the integration end points from infinite to finite values. We define

$$r_k = \sqrt{k_y^2 + k_z^2} \quad \text{and} \quad \phi_k = \tan^{-1}\left(\frac{k_z}{k_y}\right), \quad (\text{A } 2)$$

so that

$$k_r = \mathbf{k} \cdot \hat{\mathbf{e}}_r = r_k \cos(\phi_k - \phi) \quad \text{and} \quad k_\phi = \mathbf{k} \cdot \hat{\mathbf{e}}_\phi = r_k \sin(\phi_k - \phi), \quad (\text{A } 3)$$

while  $k_x$  is the same in all these coordinate systems. We see that the quantities  $k_r$  and  $k_\phi$  depend upon which  $\mathbf{x}$  position we are considering via the quantity  $\phi$ . The angle  $\phi_k$  appears in our subsequent expression for the blade normal velocity, see equation (4.2).



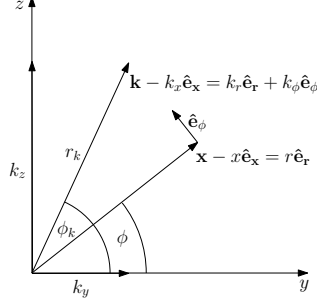


Figure 13: Re-expressing  $\mathbf{k}$  in polar form:  $k_y \hat{\mathbf{e}}_y + k_z \hat{\mathbf{e}}_z \rightarrow k_r \hat{\mathbf{e}}_r + k_\phi \hat{\mathbf{e}}_\phi$ , where polar coordinates are taken with respect to position  $\mathbf{x}$ .

We note that within the analysis of Majumdar & Peake (1998),  $\phi_k$  was set equal to  $\phi$  within the definition of  $\mathbf{A}$ . This meant that, for a particular, constant,  $\mathbf{k} = (k_x, k_y, k_z)$ , the  $\phi$  dependence within  $\mathbf{A}(\mathbf{x}; \mathbf{k})$ , as  $\mathbf{x}$  was varied, was neglected. This form of averaging means that Majumdar & Peake's original analysis cannot be immediately extended to the asymmetric case, as inclusion of the differences in the distortion amplitude  $\mathbf{A}$  as  $\phi$  varies is precisely what we are aiming to do in the asymmetric case. Hence our approach in the present paper, as described in detail in §4, involves introducing new quantities  $C_{ij}^{m,n}$  and  $D_j^{m,n}$ , in order to explicitly separate out the  $\phi$  dependence within  $\mathbf{A}$  in exponential form.

Our approach also differs from that of some authors, for example Blandeau (2011), who decompose the turbulent velocity into components with constant  $k_r$ ,  $k_\phi$  components, as opposed to constant  $k_y$ ,  $k_z$  components. Within Blandeau's framework,  $k_r$  is defined to be the component of  $\mathbf{k}$  in the  $\hat{\mathbf{e}}_r$  direction on a particular blade (at  $\phi = 0$  say), and the phase is written using the strip theory approximation

$$e^{i(k_r r + k_\phi \phi r + k_x x)}, \quad (\text{A } 4)$$

which is valid on neighbouring blades, for which  $\phi$  is small. For our purposes, as we specifically wish to account for the new  $\phi$  dependence within the velocity field due to the asymmetry of the mean flow, we need to obtain general expressions which are valid for all  $\phi$  between 0 and  $2\pi$ , hence our current approach.

## Appendix B. Polar representation of the distorted wavevector and distortion amplitude

As given in equation (2.4) the distorted wavevector  $\mathbf{l}$  is given by (summation convention assumed)

$$\mathbf{l} = k_i \nabla X_i = \left\{ \hat{\mathbf{e}}_x \frac{\partial}{\partial x} + \hat{\mathbf{e}}_y \frac{\partial}{\partial y} + \hat{\mathbf{e}}_z \frac{\partial}{\partial z} \right\} [k_x X + k_y Y + k_z Z], \quad (\text{B } 1)$$

where  $\mathbf{k}$  is the (constant) wavevector at upstream infinity. We note that  $Y$  and  $Z$  are given by  $R \cos \Phi$  and  $R \sin \Phi$  in terms of polar quantities. The most general, fully asymmetric,

forms for  $l_r$  and  $l_\phi$  are then as follows:

$$\begin{aligned}
l_r &= \mathbf{1} \cdot \hat{\mathbf{e}}_r = k_x \frac{\partial X}{\partial r} + k_\phi \left( -\sin \phi \frac{\partial(R \cos \Phi)}{\partial r} + \cos \phi \frac{\partial(R \sin \Phi)}{\partial r} \right) + \\
&\quad k_r \left( \cos \phi \frac{\partial(R \cos \Phi)}{\partial r} + \sin \phi \frac{\partial(R \sin \Phi)}{\partial r} \right), \\
l_\phi &= \mathbf{1} \cdot \hat{\mathbf{e}}_\phi = k_x \frac{1}{r} \frac{\partial X}{\partial \phi} + k_\phi \frac{1}{r} \left( -\sin \phi \frac{\partial(R \cos \Phi)}{\partial \phi} + \cos \phi \frac{\partial(R \sin \Phi)}{\partial \phi} \right) + \\
&\quad k_r \frac{1}{r} \left( \cos \phi \frac{\partial(R \cos \Phi)}{\partial \phi} + \sin \phi \frac{\partial(R \sin \Phi)}{\partial \phi} \right).
\end{aligned} \tag{B2}$$

The axial component  $l_x$  of course taking the same value as in the cartesian case.

Turning now to the distortion amplitude tensor  $A_{ij}$ , we define polar components by contracting the tensor with corresponding polar unit vectors, so that for instance  $A_{r\phi} \equiv \hat{\mathbf{e}}_r \cdot \mathbf{A} \cdot \hat{\mathbf{e}}_\phi$ , et cetera. After some algebra we find

$$\begin{aligned}
A_{\alpha x} &= \left( \delta_{\alpha x} - \frac{l_\alpha l_x}{|\mathbf{l}|^2} \right) \frac{\partial X}{\partial x} + \left( \delta_{\alpha r} - \frac{l_\alpha l_r}{|\mathbf{l}|^2} \right) \frac{\partial X}{\partial r} + \left( \delta_{\alpha \phi} - \frac{l_\alpha l_\phi}{|\mathbf{l}|^2} \right) \frac{1}{r} \frac{\partial X}{\partial \phi}, \\
A_{\alpha r} &= \left( \delta_{\alpha x} - \frac{l_\alpha l_x}{|\mathbf{l}|^2} \right) \frac{\partial X_r}{\partial x} + \left( \delta_{\alpha r} - \frac{l_\alpha l_r}{|\mathbf{l}|^2} \right) \frac{\partial X_r}{\partial r} \\
&\quad + \left( \delta_{\alpha \phi} - \frac{l_\alpha l_\phi}{|\mathbf{l}|^2} \right) \left[ \frac{\cos \phi}{r} \frac{\partial(R \cos \Phi)}{\partial \phi} + \frac{\sin \phi}{r} \frac{\partial(R \sin \Phi)}{\partial \phi} \right], \\
A_{\alpha \phi} &= \left( \delta_{\alpha x} - \frac{l_\alpha l_x}{|\mathbf{l}|^2} \right) \frac{\partial X_\phi}{\partial x} + \left( \delta_{\alpha r} - \frac{l_\alpha l_r}{|\mathbf{l}|^2} \right) \frac{\partial X_\phi}{\partial r} \\
&\quad + \left( \delta_{\alpha \phi} - \frac{l_\alpha l_\phi}{|\mathbf{l}|^2} \right) \left[ -\frac{\sin \phi}{r} \frac{\partial(R \cos \Phi)}{\partial \phi} + \frac{\cos \phi}{r} \frac{\partial(R \sin \Phi)}{\partial \phi} \right],
\end{aligned} \tag{B3}$$

where  $X_r = R \cos(\Phi - \phi)$ , and  $X_\phi = R \sin(\Phi - \phi)$ . In these expressions the suffix  $\alpha$  runs over  $x, r, \phi$ , and  $\delta_{xx} = \delta_{rr} = \delta_{\phi\phi} = 1$ , with all other values of  $\delta_{\alpha\beta}$  being zero.

### Appendix C. Definition of $D_j^{m,n}$

As outlined in §4.1, it is helpful in the analysis to define the cartesian vector  $D_j^{m,n} \equiv N_i C_{ij}^{m,n}$ . To compute  $D_j^{m,n}$  we substitute the ‘mixed suffices’ quantities  $A_{xj}$ ,  $A_{rj}$ ,  $A_{\phi j}$  (for  $j = x, y, z$ ) in terms of the polar  $\mathbf{A}$  components given in Appendix B above, into the left hand side of equation (4.4). For example

$$\begin{aligned}
[\hat{\mathbf{e}}_x \cdot \mathbf{A} \cdot \hat{\mathbf{e}}_y] e^{ik_x X} J_n(r_k R) e^{in\Phi} &= \{ [\hat{\mathbf{e}}_x \cdot \mathbf{A} \cdot \hat{\mathbf{e}}_r] \cos \phi - [\hat{\mathbf{e}}_x \cdot \mathbf{A} \cdot \hat{\mathbf{e}}_\phi] \sin \phi \} e^{ik_x X} J_n(r_k R) e^{in\Phi} \\
&= \sum_{m=-\infty}^{\infty} \left[ C_{xr}^{m,n} \cos \phi - C_{x\phi}^{m,n} \sin \phi \right] e^{im\phi} \\
&= \frac{1}{2} \sum_{m=-\infty}^{\infty} \left\{ \left( C_{xr}^{m-1,n} + i C_{x\phi}^{m-1,n} \right) + \left( C_{xr}^{m+1,n} - i C_{x\phi}^{m+1,n} \right) \right\} e^{im\phi}.
\end{aligned} \tag{C1}$$

Here we see that  $m \pm 1$  suffices have arisen due to the extra  $\cos \phi$ ,  $\sin \phi$  factors.

Contracting  $\mathbf{N}$  with the relevant components of  $C_{ij}^{m,n}$  thus gives rise to the following

full definitions

$$\begin{aligned}
 D_x^{m,n}(x, r; k_x, r_k, \phi_k) &\equiv \left[ \sin \beta C_{xx}^{m,n} + \cos \beta C_{\phi x}^{m,n} \right], \\
 D_y^{m,n}(x, r; k_x, r_k, \phi_k) &\equiv \frac{1}{2} \left[ \sin \beta \left\{ \left( C_{xr}^{m-1,n} + i C_{x\phi}^{m-1,n} \right) + \left( C_{xr}^{m+1,n} - i C_{x\phi}^{m+1,n} \right) \right\} + \right. \\
 &\quad \left. \cos \beta \left\{ \left( C_{\phi r}^{m-1,n} + i C_{\phi\phi}^{m-1,n} \right) + \left( C_{\phi r}^{m+1,n} - i C_{\phi\phi}^{m+1,n} \right) \right\} \right], \\
 D_z^{m,n}(x, r; k_x, r_k, \phi_k) &\equiv \frac{1}{2} \left[ \sin \beta \left\{ \left( -i C_{xr}^{m-1,n} + C_{x\phi}^{m-1,n} \right) + \left( i C_{xr}^{m+1,n} + C_{x\phi}^{m+1,n} \right) \right\} + \right. \\
 &\quad \left. \cos \beta \left\{ \left( -i C_{\phi r}^{m-1,n} + C_{\phi\phi}^{m-1,n} \right) + \left( i C_{\phi r}^{m+1,n} + C_{\phi\phi}^{m+1,n} \right) \right\} \right]. \tag{C 2}
 \end{aligned}$$

where the  $C_{ij}^{m,n}$  terms on the right hand sides have the same arguments as the  $D_j^{m,n}$  terms on the left hand sides. When substituting back to obtain equation (4.7) we rewrite the expression for  $D_j^{m,n}$  with a general argument in terms of its value with  $\phi_k$  set to zero, as follows

$$D_j^{m,n}(x, r; k_x, r_k, \phi_k) = e^{-im\phi_k} D_j^{m,n}(x, r; k_x, r_k, 0) + E. \tag{C 3}$$

The extra terms within  $E$  include additional  $e^{\pm i\phi_k}$  factors. However, when the full integral over all  $\mathbf{k}$  is taken these terms are found to integrate to zero, and thus  $E$  does not appear within the expressions in this paper.

## Appendix D. Full expression for radiated sound

$$\begin{aligned}
 \hat{P}(\sigma_0, \theta', \phi', \omega) &= \rho_0^2 \frac{B^2}{4\pi^2 U_\infty} \frac{1}{4\sigma_0^2 (1 - M \cos \theta)^2} \\
 &\quad \sum_{l,m,m'} \int_{r'_s, x'_s} [J_{m+lB}(\gamma'_0 r'_s)]^* [W(r'_s) \gamma^m(x'_s, r'_s; \omega)]^* \\
 &\quad \left[ \frac{i\omega \cos \theta' \sin \beta(r'_s)}{c_0 (1 - M \cos \theta)} - \frac{i(m+lB) \cos \beta(r'_s)}{r'_s} \right] \\
 &\quad \exp \left\{ \frac{-i\omega \cos \theta' x'_s}{c_0 (1 - M \cos \theta)} + i(m+lB) \frac{[x'_s - x_0(r'_s)] \tan \beta(r'_s)}{r'_s} + ilB\phi_0(r'_s) \right\} \\
 &\quad \int_{r'_t, x'_t} J_{m'+lB}(\gamma'_0 r'_t) W(r'_t) \gamma^{m'}(x'_t, r'_t; \omega) \\
 &\quad \left[ -\frac{i\omega \cos \theta' \sin \beta(r'_t)}{c_0 (1 - M \cos \theta)} + \frac{i(m'+lB) \cos \beta(r'_t)}{r'_t} \right] \\
 &\quad \exp \left\{ \frac{i\omega \cos \theta' x'_t}{c_0 (1 - M \cos \theta)} - i(m'+lB) \frac{[x'_t - x_0(r'_t)] \tan \beta(r'_t)}{r'_t} - ilB\phi_0(r'_t) \right\} \\
 &\quad \sum_{n,n'} \int_{\mathfrak{R}} [D_j^{m,n}(x_0(r'_s), r'_s; k_x, r_k, 0)]^* D_k^{m',n'}(x_0(r'_t), r'_t; k_x, r_k, 0) \\
 &\quad \left[ \int_0^{2\pi} e^{i(m+n-m'-n')\phi_k} S_{kl}^\infty(\mathbf{k}) d\phi_k \right] r_k dr_k dr'_t dx'_t dr'_s dx'_s e^{i(m'-m)(\phi' - \frac{\pi}{2})}. \tag{D 1}
 \end{aligned}$$

For the case of asymmetric flow 1,  $\theta'$  and  $\phi'$  are replaced by  $\theta$  and  $\phi$  everywhere.

When calculating the radiated sound level numerically for a given frequency  $\omega$  it is necessary to restrict the infinite sums over the  $l, m, n$  indices to the dominant terms only in order to reduce the computational intensity of calculations.

Considering first the summation over the  $l$  index we find that the most significant terms arise from those  $l$  values which result in  $k_x = \omega - lB\Omega/U_\infty$  being as close to zero as possible, due to the sharp decay of  $S_{kl}^\infty$  as  $|\mathbf{k}|$  increases. For values of  $\omega$  in the ranges

of interest to us (0 - 2 BPF) we therefore take values of  $l$  centred on 0, 1 or 2. The difference between using a total of 3 or 5  $l$  values is found to be negligible and so we take the total number of  $l$  values included in the sum,  $n_l$ , to be 3 in all our calculations.

Next, we include an odd number of  $m$  values centred on  $-lB$ , due to the decay of the  $J_{m+lB}$  term (within the Green's function) as the order increases. This sum is slightly more sensitive to the total number of  $m$  values,  $n_m$ , as the decay of the Bessel functions is not as rapid as that of  $S_{kl}^\infty$ . We find that setting  $n_m = 7$  in our calculations for the present paper gives sufficiently accurate results.

Finally, we choose values of  $n$  centred on zero, again due to the decay of a Bessel function, in this case the  $J_n$  term within  $C_{ij}^{m,n}$ . We find that in all cases nine or fewer values of  $n$  are significant contributors to the total sum. Including  $n = -4, \dots, 4$  is sufficient for the parameters under consideration here. We also find that setting  $n = n'$  gives sufficiently accurate results which are very close to the  $n \neq n'$  case, as well as significantly speeding up the numerics. A final point to note is that in the high distortion case fewer terms are typically needed for convergence than in the low distortion case.

When calculating the radiated sound integrated over a shell in the twin disk (asymmetric flow 1) case, the expression is simplified as the integral over  $\phi$  leads to a  $\delta_{mm'}$  term, and so we can set  $m = m'$ . This cannot be done in the incidence (asymmetric flow 2) case as  $\phi'$  appears within the expressions for  $\theta'$ . The time average acting upon  $\exp(ilBt)$  and  $\exp(-il'Bt)$  leads to a  $\delta_{ll'}$  term, hence the summation over  $l$  only.

When calculating the spectral power numerically we choose a discrete set of  $r'_s, r'_t$  values (typically around 6 values) and the integrand is then evaluated for all pairs of  $r'_s, r'_t$  and summed using the trapezium rule, first over  $r'_s$  then over  $r'_t$ . For a particular pair of  $r'_s, r'_t$ , the integral over  $r_k$  does not converge with an infinite upper limit for  $r_k$  and we are able to achieve convergence by using the limited range for this integral given earlier in (4.13). Since  $R$  and  $\partial R/\partial r$  also differ for  $r'_s$  and  $r'_t$  we have a choice as to whether to take the inner or outer of each limit. We use the outer limits, thus using the larger value of  $R$  and the smaller value of  $\partial R/\partial r$ , although in fact there is little difference if the inner limits are used. A final approximation is that the  $C_{ij}^{m,n}$  terms are calculated via a fast Fourier Transform, using  $A_{ij}$  values calculated at a discrete set of  $\phi$  values (typically 8 values).

One final point is to note that a series of partial validation tests were carried out at each stage of the computation of (D 1). First, the rapid distortion theory calculation was validated, at least in the axisymmetric case, by comparing our distorted spectra with results obtained by Majumdar & Peake (1998). Second, the implementation of LINSUB for the blade response was checked by comparing with standard results published in Smith (1973) and elsewhere. Third, the noise radiation results were checked in the limit of weak asymmetry for consistency with the axisymmetric noise results of Majumdar & Peake (1998).

## REFERENCES

- ALEXANDER, N., DEVENPOR, W., MORTON, M.A. & GLEGG, S.A.L. 2013 Noise from a rotor ingesting a planar turbulent boundary layer. *Proc. of 19th AIAA/CEAS Aeroacoustics Conference* (AIAA 2013-2285).
- AMIET, R. K. 1975 Acoustic radiation from an airfoil in a turbulent stream. *Journal of Sound and Vibration* **41** (4), 407–420.
- AMIET, R. K., SIMONICH, J. C. & SCHLINKER, R. H. 1990 Rotor noise due to atmospheric turbulence ingestion. Part II: Aeroacoustic results. *Journal of Aircraft* **27** (1), 15–22.
- AYTON, L.J. & PEAKE, N. 2014 On high-frequency sound generation by gust-aerofoil interaction in shear flow. *Journal of Fluid Mechanics* **Submitted**.

- BLANDEAU, V. P. 2011 Aerodynamic broadband noise from contra-rotating open rotors. PhD thesis, University of Southampton.
- CARGILL, A. M. 1993 A theory for fan unsteady distortion noise. Theoretical Science Group Report TSG0675. Rolls-Royce plc.
- CRIGHTON, D.G. & PARRY, A.B. 1991 Asymptotic theory of propeller noise part ii: supersonic single-rotation propeller. *AIAA Journal* **29**, 2031–2037.
- CUMPSTY, N. A. & LOWRIE, B. W. 1974 The cause of tone generation by aeroengine fans at high subsonic speeds and the effect of forward speed. *Journal of Engineering for Power* **96** (3), 228–234.
- DOWLING, A. P. & FLOWCS WILLIAMS, J. E. 1983 *Sound and sources of sound*. Ellis Horwood.
- FLOWCS WILLIAMS, J. E. & HAWKINGS, D. L. 1969 Sound generation by turbulence and surfaces in arbitrary motion. *Phil. Trans. Roy. Soc. Lond* **265**, 321–342.
- GLEGG, S.A.L., DEVENPORT, W. & ALEXANDER, N. 2014 Broadband rotor noise predictions using a time domain approach. *J. Sound Vib.* (submitted).
- GLEGG, S.A.L., KAWASHIMA, E., LACHOWSKI, F., DEVENPORT, W. & ALEXANDER, N. 2013 Inflow distortion noise in a non axisymmetric flow. *Proc. of 19th AIAA/CEAS Aeroacoustics Conference* (AIAA 2013-2286).
- GLEGG, S. A. L. & JOCHAULT, C. 1998 Broadband self-noise from a ducted fan. *AIAA Journal* **36** (8), 1387–1395.
- GOLDSTEIN, M. E. 1978a Characteristics of the unsteady motion on transversely sheared mean flows. *Journal of Fluid Mechanics* **84**, 305–329.
- GOLDSTEIN, M. E. 1978b Unsteady vortical and entropic distortions of potential flows round arbitrary obstacles. *Journal of Fluid Mechanics* **89** (3), 433–468.
- GRADSHTEYN, I. S. & RYZHIK, I. M. 1980 *Table of integrals, series and products*.
- HANSON, D. B. 1974 Spectrum of rotor noise caused by atmospheric turbulence. *Journal of the Acoustical Society of America* **56** (1), 110–126.
- HANSON, D. B. 1995 Sound from a propeller at angle of attack: a new theoretical viewpoint. *Proc. Mathematical and Physical Sciences* **449** (1936), 315–328.
- HANSON, D. B. 2001 Theory for broadband noise of rotor and stator cascades with inhomogeneous inflow turbulence including effects of lean and sweep. NASA contractor report. United Technologies Corporation.
- HOMICZ, G. F. & GEORGE, A. R. 1974 Broadband and discrete frequency radiation from subsonic rotors. *Journal of Sound and Vibration* **36** (2), 151–177.
- HOUGH, G. R. & ORDWAY, D. E. 1965 pp. 317–336.
- HUNT, J. C. R. 1973 A theory of turbulent flow round two-dimensional bluff bodies. *Journal of Fluid Mechanics* **61** (4), 625–706.
- KINGAN, M. J. & MCALPINE, A. 2010 Propeller tone scattering. *Proc. of 17th International Congress on Sound and Vibration*.
- LIGHTHILL, M. J. 1956 Drift. *Journal of Fluid Mechanics* **1**, 31–53.
- LLOYD, A. E. D. 2009 Rotor stator interaction noise. PhD thesis, University of Cambridge.
- MAJUMDAR, S. J. 1996 Unsteady distortion noise. PhD thesis, University of Cambridge.
- MAJUMDAR, S. J. & PEAKE, N. 1998 Noise generation by the interaction between ingested turbulence and a rotating fan. *Journal of Fluid Mechanics* **359**, 181–216.
- MANI, R. 1971 Noise due to interaction of inlet turbulence with isolated stators and rotors. *Journal of Sound and Vibration* **17** (2), 251–260.
- PARRY, A.B. & CRIGHTON, D.G. 1989 Asymptotic theory of propeller noise part i: subsonic single-rotation propeller. *AIAA Journal* **27**, 1184–1190.
- PARRY, A. B. 1988 Theoretical prediction of counter-rotating propeller noise. PhD thesis, University of Leeds.
- PATERSON, R. W. & AMIET, R. K. 1982 Noise of a model helicopter rotor due to ingestion of isotropic turbulence. *Journal of Sound and Vibration* **85** (4), 551–577.
- PEAKE, N. & PARRY, A. B. 2012 Modern challenges facing turbomachinery aeroacoustics. *Annual Review of Fluid Mechanics* **44**, 227–248.
- POSSON, H., BERIOT, H. & MOREAU, S. 2013 On the use of an analytical cascade response function to predict sound transmission through an annular cascade. *J. Sound Vib.* **332**, 3706–3739.

- POSSON, H., MOREAU, S., BERIOT, H., DE L'EPINE, Y. B. & SCHRAM, C. 2010 Prediction of sound transmission through an annular cascade using an analytical cascade response function. *Proc. of 16th AIAA/CEAS Aeroacoustics Conference* (AIAA 2010-4030).
- ROBISON, R. A. V. 2011 Turbulence ingestion noise of open rotors. PhD thesis, University of Cambridge.
- SHARLAND, I. J. 1964 Sources of noise in axial flow fans. *Journal of Sound and Vibration* **1** (3), 302–322.
- SIMONICH, J. C., AMIET, R. K., SCHLINKER, R. H. & GREITZER, E. M. 1990 Rotor noise due to atmospheric turbulence ingestion. Part I: Fluid mechanics. *Journal of Aircraft* **27** (1), 7–14.
- SMITH, B. A. 1985 McDonnell Douglas nears commitment to fly propfan on MD-80 testbed. *Aviation Week and Space Technology* **122** (20), 32–33.
- SMITH, S. N. 1973 Discrete frequency sound generation in axial flow turbomachines. Aeronautical Research Council Reports and Memoranda 3709. Ministry of Defence.
- WHITEHEAD, D. S. 1987 Classical two-dimensional methods. Manual on Aeroelasticity in Axial-Flow Turbomachinery AGARD-AG-298 Vol. 1 ISBN 92-835-1543-9. Advisory Group for Aerospace Research and Development.
- WILSON, D. K., BRASSEUR, J. G. & GILBERT, K. E. 1999 Acoustic scattering and the spectrum of atmospheric turbulence. *The Journal of the Acoustical Society of America* **105** (1), 30–34.
- WILSON, D. K. & THOMSON, D. W. 1994 Acoustic propagation through anisotropic, surface-layer turbulence. *The Journal of the Acoustical Society of America* **96** (2), 1080–1095.